



# VCU

Virginia Commonwealth University  
VCU Scholars Compass

---

Theses and Dissertations

Graduate School


---

2015

## Characterization of a Novel Protease in *Staphylococcus aureus*

Adam L. Johnson  
*Virginia Commonwealth University*

Follow this and additional works at: <https://scholarscompass.vcu.edu/etd>

 Part of the [Bacteria Commons](#), [Bacterial Infections and Mycoses Commons](#), [Biochemistry Commons](#), [Enzymes and Coenzymes Commons](#), [Microbiology Commons](#), and the [Molecular Biology Commons](#)

© The Author

---

Downloaded from

<https://scholarscompass.vcu.edu/etd/3943>

This Thesis is brought to you for free and open access by the Graduate School at VCU Scholars Compass. It has been accepted for inclusion in Theses and Dissertations by an authorized administrator of VCU Scholars Compass. For more information, please contact [libcompass@vcu.edu](mailto:libcompass@vcu.edu).

© Adam Lee Johnson 2015  
All Rights Reserved

CHARACTERIZATION OF A NOVEL PROTEASE IN *STAPHYLOCOCCUS AUREUS*

A thesis submitted in partial fulfillment of the requirements for the degree of Master of Science at Virginia Commonwealth University.

by

ADAM LEE JOHNSON  
B.S., Old Dominion University, 2012

Director: Dr. Gail E. Christie, Ph.D.  
Professor, Department of Microbiology and Immunology  
Virginia Commonwealth University  
Richmond, Virginia

Virginia Commonwealth University  
Richmond, Virginia  
July 2015

## Acknowledgement

I would like to first and foremost thank my advisor, Dr. Gail Christie, for her support and guidance throughout this work and in my graduate career. I would also like to thank my committee members, Dr. William Barton and Dr. Darrell Peterson, for their expertise and indispensable contributions to this work. Finally, I would like to thank my lab mates, Dr. Erin Wall, for her groundwork for this project, and Laura Klenow, for her help with experiments and presentations and for putting up with me on a daily basis.

## Table of Contents

	Page
Acknowledgements.....	ii
List of Tables.....	v
List of Figures.....	vi
List of Abbreviations.....	viii
Abstract.....	xii
Chapter	
1. Introduction.....	1
2. Materials and Methods.....	17
I. Bacterial Culture.....	17
II. DNA Manipulations.....	17
III. Generating Prp Mutants.....	19
a. Isolation of Genomic DNA.....	19
b. Polymerase Chain Reaction (PCR).....	20
c. Agarose Gel Electrophoresis.....	22
d. Construction of Expression Plasmids.....	23
e. Bacterial Transformation.....	23
IV. Expression and Purification of Recombinant Proteins.....	25

a. Recombinant Protein Overexpression via Autoinduction Culture.....	25
b. Purification of Recombinant Proteins.....	26
c. Cleavage of the His <sub>6</sub> -SUMO Tag from Prp.....	27
d. Sodium Dodecyl Sulfate-Polyacrylamide Gel Electrophoresis (SDS-PAGE).....	28
e. Bradford Protein Quantification Assay.....	29
V. Fast Protein Liquid Chromatography.....	30
VI. Fluorogenic Peptide Cleavage Assay, Generating a Standard Curve and Determining the Extent of Assay Completion, and Data Analysis.....	30
a. Fluorogenic Peptide Cleavage Assay.....	30
b. Generating a Standard Curve and Determining the Extent of Assay Completion.....	33
c. Data Analysis.....	33
3. Expression and Purification of Wild-type Prp and Generation of Active-site Mutants.....	37
4. Standardization of a Fluorogenic Peptide Cleavage Assay.....	44
5. Enzyme Kinetics of Wild-type Prp, Competition Assays with Alternative Substrates, and Activity of Active-site Mutants.....	52
6. Discussion.....	59
References.....	71
Vita.....	75

## List of Tables

	Page
Table 1: Bacterial strains and plasmids used in this study.....	18
Table 2: Primers used in this study.....	21
Table 3: Synthetic peptides used in this study.....	31
Table 4: Comparing the kinetics of sequence-specific proteases.....	64

## List of Figures

	Page
Figure 1.1: The bacterial ribosome.....	4
Figure 1.2: Binding sites of antibiotics on the bacterial ribosome.....	7
Figure 1.3: Tetrahedral intermediates formed during peptide cleavage.....	9
Figure 1.4: Ribosomal protein L27 and tRNA at the PTC in <i>E. coli</i> .....	11
Figure 1.5: L27 and Prp phylogeny across major bacterial phyla.....	12
Figure 1.6: An L27 complementation system.....	14
Figure 1.7: Diagram of the fluorogenic peptide cleavage assay.....	15
Figure 2.1: Standard curve for converting raw RFU values from Prp assays to concentration of fluorogenic substrate cleaved.....	34
Figure 2.2: Comparing absolute RFU values between completed reactions with trypsin and Prp.....	35
Figure 3.1: SDS-PAGE gel of His <sub>6</sub> -tagged Ulp1 and Prp from P10 column.....	39
Figure 3.2: SDS-PAGE gel of Prp pre- and post-purification.....	41
Figure 3.3: Active-site mutations introduced into Prp.....	42
Figure 4.1: Effect of pH.....	46
Figure 4.2: Effect of DTT.....	47
Figure 4.3: Effect of EDTA.....	48



Figure 4.4: Effect of NaCl.....	50
Figure 4.5: Additive effects of pH 7.0 buffer with DTT and EDTA.....	51
Figure 5.1: Michaelis-Menten plot of Prp kinetics data.....	54
Figure 5.2: Initial velocity and percent inhibition of assays with competitive peptides.....	55
Figure 5.3: Initial velocity and percent activity of Prp active-site mutants.....	57
Figure 5.4: Percent activity of S38A mutant.....	58
Figure 6.1: Prp model with substrate docked.....	66
Figure 6.2: Atomic resolution model of Prp active site with substrate docked.....	68

## List of Abbreviations

°C	degrees Celsius
%v/v	volume/volume percent
%w/v	weight/volume percent
amp	ampicillin
APS	ammonium persulfate
AU	absorbance units
<i>B. subtilis</i>	<i>Bacillus subtilis</i>
bp	base pair
BSA	bovine serum albumin
cAMP	cyclic adenosine monophosphate
CA-MRSA	community-acquired methicillin-resistant <i>Staphylococcus aureus</i>
chl	chloramphenicol
CRP	cAMP receptor protein
DMSO	dimethyl sulfoxide
DNA	deoxyribonucleic acid
dNTP	deoxyribonucleotide triphosphate
DTT	dithiothreitol

<i>E. coli</i>	<i>Escherichia coli</i>
EDTA	ethylenediaminetetraacetic acid
$E_T$	total enzyme
EtBr	ethidium bromide
FPLC	fast protein liquid chromatography
g	gram
g/L	gram per liter
gDNA	genomic DNA
gly	glycine
His <sub>6</sub>	hexahistidine
HPLC	high-performance liquid chromatography
$k_{cat}$	turnover number
$K_m$	Michaelis-Menten constant
L	liter
L27	large ribosomal protein L27
LB	Luria-Bertani/lysogeny broth
M	molar
mA	milliamperes
mg	milligram
mg/ml	milligram per milliliter
min	minute
ml	milliliter
ml/L	milliliter per liter

ml/min	milliliter per minute
mm	millimeter
mM	millimolar
MRSA	methicillin-resistant <i>Staphylococcus aureus</i>
MSCRAMM	microbial surface components recognizing adhesive matrix molecules
MW	molecular weight
MWCO	molecular weight cut-off
NaCl	sodium chloride
ng	nanogram
nm	nanometer
PCR	polymerase chain reaction
Prp	phage-related ribosomal protease
psi	pounds per square inch
PTC	peptidyl transferase center
rpm	revolutions per minute
s	second
<i>S. aureus</i>	<i>Staphylococcus aureus</i>
SaPI	<i>Staphylococcus aureus</i> pathogenicity island
SDS	sodium dodecyl sulfate
SDS-PAGE	sodium dodecyl sulfate - protein acrylamide gel electrophoresis
SOC	super optimal broth with catabolite repression

SUMO	small ubiquitin-like modifier
TAE	tris-acetate-EDTA
TEMED	tetramethylethylenediamine
TEV NIa	Tobacco Etch Virus nuclear inclusion A protease
$T_m$	melting temperature
tRNA	transfer RNA
$\mu\text{g}$	microgram
$\mu\text{l}$	microliter
Ulp1	ubiquitin-like protein-specific protease 1
$\mu\text{m}$	micrometer
$\mu\text{M}$	micromolar
UV	ultraviolet
V	volts
$V_{\text{max}}$	maximum velocity
WT	wild-type
X	times
X g	times the force of gravity

## Abstract

### CHARACTERIZATION OF A NOVEL PROTEASE IN *STAPHYLOCOCCUS AUREUS*

By Adam Lee Johnson

A thesis submitted in partial fulfillment of the requirements for the degree of Master of Science at Virginia Commonwealth University.

Virginia Commonwealth University, 2015

Major Director: Gail E. Christie, Ph.D.  
Professor, Department of Microbiology and Immunology

A newly discovered cysteine protease, Prp, has been shown to perform an essential, site-specific cleavage of ribosomal protein L27 in *Staphylococcus aureus*. In Firmicutes and related bacteria, ribosomal protein L27 is encoded with a conserved N-terminal extension that must be removed to expose residues critical for ribosome function. Uncleavable and pre-cleaved variants were unable to complement an L27 deletion in *S. aureus*, indicating that this N-terminal processing event is essential and likely plays an important regulatory role. The gene encoding the responsible protease (*prp*) has been

shown to be essential, and is found in all organisms encoding the N-terminal extension of L27. Cleavage of L27 by Prp represents a new target for potential antibiotic therapy. In order to characterize this protease, Prp has been overexpressed and purified. Using an assay we have developed, based on cleavage of a fluorogenic peptide derived from the conserved L27 cleavage sequence, we have undertaken an analysis of the enzyme kinetics and substrate specificity for Prp cleavage and tested predictions made based on a structural model using active-site mutants.

## Chapter 1

### Introduction

*Staphylococcus aureus* is a Gram-positive bacterium and is a commensal inhabitant of the skin and mucosal epithelia; it is estimated that approximately 20% of individuals are nasal carriers. This colonization provides a reservoir of bacteria with the ability to cause infection in cases of a breakdown in host defenses, such as loss of the skin barrier (wounds, surgery, etc.) or underlying disease (diabetes, AIDS, etc.). Upon infection, *S. aureus* can cause a wide range of disease, including skin, respiratory, bone, and endovascular disorders. More life-threatening conditions, such as bacteremia, endocarditis, metastatic infections, and sepsis, are also a major concern. These diseases can be further complicated by the presence of virulence factors, including surface proteins (microbial surface components recognizing adhesive matrix molecules—MSCRAMMs), capsules, hydrolytic enzymes (proteases, lipases, nucleases, etc.), and toxins (leukocidins, enterotoxins, exfoliative toxins, alpha-toxin, toxic shock syndrome toxin-1, etc.), which help the bacterium adapt to and evade the host immune system (Lowy, 1998; Wertheim et al., 2005, Gordon & Lowy, 2008; Chambers & DeLeo, 2009; Reyes-Robles et al., 2014).

*S. aureus* is naturally susceptible to practically all antibiotics. However, it has rapidly developed mechanisms of antibiotic resistance through horizontal gene transfer,



chromosomal mutations, and antibiotic selection (Chambers & DeLeo, 2009). The development of antibiotic resistance in *S. aureus* began shortly after the introduction of penicillin in the 1940s, whereupon strains carrying the gene for  $\beta$ -lactamase first emerged in health-care settings then spread to the community. In 1961, methicillin was introduced and used to treat patients with penicillin-resistant *S. aureus* infections. However, methicillin-resistant strains (MRSA) were isolated later that same year. Like the penicillin-resistant strains, methicillin-resistant strains spread from hospitals to the community, although, surprisingly, community cases also appeared in patients with no prior hospitalizations. The increasing prevalence of MRSA and community-acquired MRSA (CA-MRSA) led to a dramatic increase in the use of vancomycin, and predictably, strains with intermediate or complete resistance to vancomycin have since been isolated (Lowy, 2003).

Currently, antibiotic resistance is found in all major pathogens and to all classes of antibiotics. Most available antibiotics are based on the chemical scaffolds of natural products that were discovered over 40 years ago. These scaffolds form the basis for a drug's activity, while their surrounding chemical groups are altered in subsequent generations to circumvent resistance or make other improvements to the drug. Recently, only two new classes of broad-spectrum antibiotics have been developed and approved: the oxazolidinones (linezolid) and the lipopeptide antibiotic daptomycin (Fischbach & Walsh, 2009; Cole, 2014).

Antibiotics target essential metabolic processes of bacteria. The main classes of antibiotics have only five targets: the ribosome, cell wall synthesis, RNA polymerase, metabolic enzymes, and DNA topoisomerase. The effects of antibiotics on these targets

can directly kill the bacteria or inhibit their growth, allowing the immune system to clear the infection. The development of antibiotic resistance is not a new phenomenon. Bacteria have evolved alongside organisms that naturally produce antibiotics and, to survive, bacteria have had to develop a variety of antibiotic resistance mechanisms. These mechanisms can include inactivation of the drug, modification of the drug target, modification of the permeability of the cell wall, overproduction of the target, or bypass of the inhibited metabolic steps (Coates et al., 2002).

### Bacterial Ribosomes

Among the first antibiotics discovered from natural sources were some found to target the ribosome (Bush, 2011). Ribosomes are the site of protein synthesis inside cells. They are molecular machines composed of ribosomal RNA (rRNA) and proteins, which assemble to form a ribonucleoprotein complex (Figure 1.1). This complex is composed of a small subunit (30S) and a large subunit (50S) that come together to form a functional (70S) particle. The 30S subunit consists of 16S rRNA along with 21 proteins (S1-21), while the 50S subunit is composed of 23S rRNA, 5S rRNA, and 33 proteins (L1-36). Assembly of the ribosome is complex and highly organized; however, all of the necessary information is encoded within the rRNA and proteins themselves. Ribosomal RNA is synthesized as a single transcript, which is processed into separate rRNAs (23S, 16S, and 5S) by approximately five nucleases (RNase III, E, T, G, and one unidentified). These rRNAs can be modified at conserved and functionally important regions, which can influence both ribosome structure and function. The initial steps of ribosome assembly involve rRNA folding, which is guided along by ribosomal protein

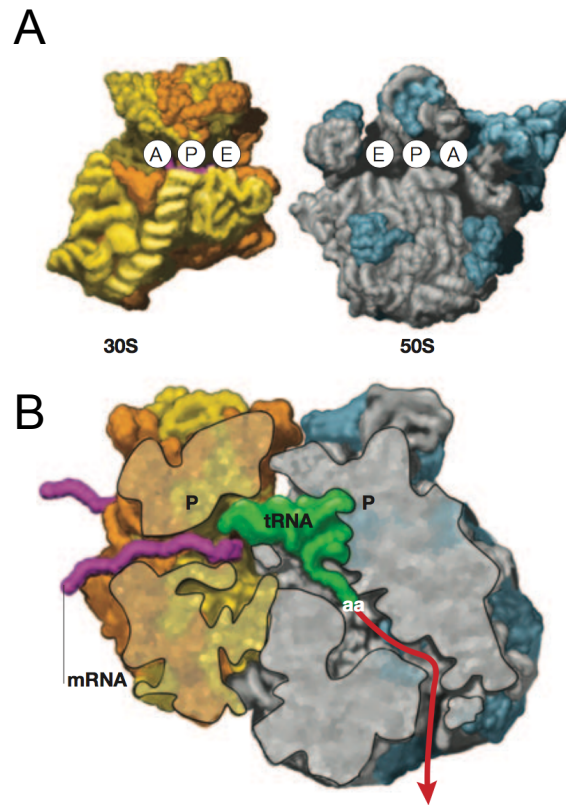


**Figure 1.1: The bacterial ribosome.**

(A) Diagrams of the 30S and 50S subunits from *Thermus thermophilus*. The backbone of rRNA is shown in yellow and grey and ribosomal proteins at the interfaces of the subunits are shown in bronze and blue. The A-, P-, and E-sites are labeled on each subunit. (B) A cross-section of the ribosome with a tRNA at the P-site. Messenger RNA is shown in purple and the polypeptide chain exit tunnel is shown as a red arrow.

Reprinted from *Nature Reviews-Microbiology*, 3, Poehlsgaard, J., Douthwaite, S., The bacterial ribosome as a target for antibiotics, 870-881, (2005), with permission from Nature Publishing Group.

binding. These proteins bind in a hierarchical manner and induce and stabilize structural changes. Many assembly factors, such as chaperones, maturation factors, and GTPases, also facilitate proper rRNA folding and protein-RNA interactions, or serve as checkpoint sensors during assembly (which is more important for the larger 50S particle). Ribosome assembly thus involves a series of rRNA conformational changes and protein-binding events and can proceed through various pathways with different assembly intermediates (Shajani et al., 2011).

The function of ribosomes is to translate the information encoded in messenger RNA (mRNA) into the amino acid sequence of proteins. The 30S subunit associates with mRNA during translation initiation and contains the decoding site where the three-nucleotide codons in the mRNA are matched with their corresponding aminoacylated transfer RNAs (tRNA). Initiation occurs when a start codon is positioned at the peptidyl site (P site) and interacts with an initiator tRNA carrying methionine. The 50S subunit, which carries the peptidyl transferase center (the catalytic site of peptide bond formation; PTC), then associates with the 30S subunit, forming the functional ribosome. A second codon at the acceptor site (A site) is matched with its corresponding aminoacyl-tRNA and a conformational change occurs, placing the aminoacyl end of the tRNA at the peptidyl transferase center, where a peptide bond is formed between the methionine and second amino acid. This moves the ribosome one codon further down the mRNA, placing the initiator tRNA at the exit site (E site) and the tRNA holding the dipeptide in the P site. The uncharged tRNA then exits the ribosome, while the acceptor site is open to receive the next charged tRNA. This process repeats until a stop codon

is reached and the polypeptide is released from the exit tunnel on the back of the ribosome (Poehlsgaard & Douthwaite, 2005).

Many antibiotics that target the ribosome are still in use today, such as aminoglycosides, tetracyclines, and macrolides (Bush, 2011). Most antibiotics that target the ribosome target the active regions of the 30S and 50S subunits (Figure 1.2). Antibiotics that bind to the 30S subunit—tetracyclines, spectinomycin, and aminoglycosides—interfere directly with mRNA decoding by causing misincorporation of amino acids, blocking binding of tRNA at the A-site, or inhibiting translocation. The larger 50S subunit is targeted at three main regions, causing interference with GTP hydrolysis, peptidyl transfer, and polypeptide channeling through the exit tunnel. The 50S subunit is targeted by a variety of antibiotics, including macrolides, lincosamides, streptogramins, chloramphenicol, puromycin, and oxazolidinones. Most of the antibiotics that target the ribosome have been found to bind at relatively few, overlapping sites (Poehlsgaard & Douthwaite, 2005; Hermann, 2005).

### Proteases

Proteases are enzymes that hydrolyze the peptide bonds between amino acids in proteins. They are one of the most abundant classes of enzymes and have been identified in almost all organisms. Proteases play a role in most biological pathways and networks, including cell-cycle progression; cell signaling, proliferation, and death; protein trafficking; and the immune response. Due to their ubiquity, they have been implicated in many diseases, such as coagulopathies, inflammation, degenerative

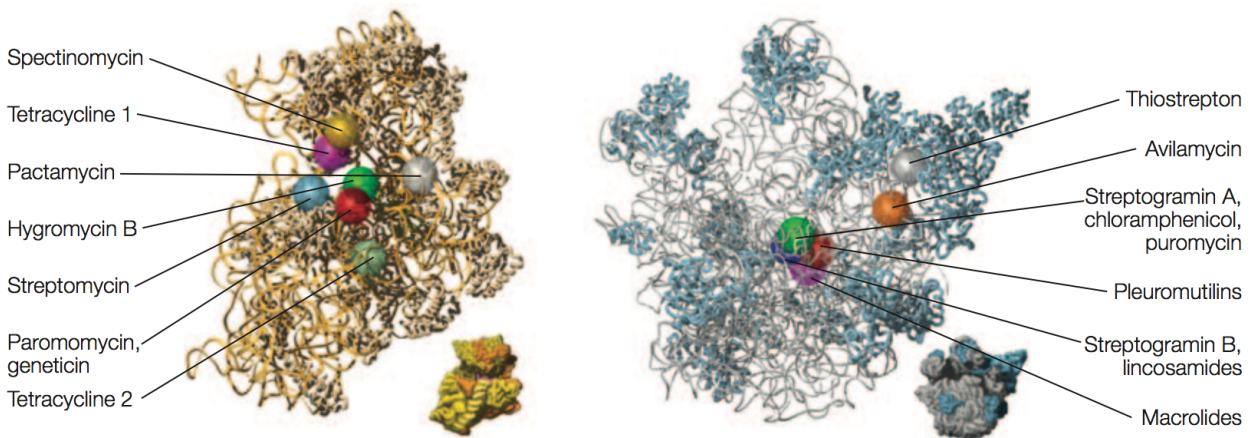


**Figure 1.2: Binding sites of antibiotics on the bacterial ribosome.**

The 30S subunit of *Thermus thermophilus* is shown on the left and the 50S subunit is on the right. Binding sites are shown as space-filling balls. Ribosomal RNA is shown as yellow and grey and ribosomal proteins are shown in bronze and blue.

Reprinted from *Nature Reviews-Microbiology*, 3, Poehlsgaard, J., Douthwaite, S., The bacterial ribosome as a target for antibiotics, 870-881, (2005), with permission from Nature Publishing Group.

diseases, cancer, and infectious disease, which also makes them important drug targets. Protease inhibiting drugs are currently in use for coagulation disorders, hypertension, HIV infection, cancer, and diabetes. It is estimated that 5-10% of all currently pursued drug targets are proteases (Drag & Salvesen, 2010; Deu et al., 2012).

There are seven classes of proteases (aspartate, glutamate, cysteine, metalloproteases, serine, threonine, and asparagine peptide lyases) that are classified with respect to their catalytic mechanism (Figure 1.3). Serine, cysteine, and threonine proteases use nucleophilic amino-acid side chains at the active site to catalyze hydrolysis through covalent intermediates, whereas aspartate, glutamate, and metalloproteases carry out hydrolysis using an activated water molecule generated by a carboxylic acid group or metal ion. Due to the highly conserved mechanisms among the different classes of proteases, target specificity has been a major obstacle in the development of protease inhibitors. Many proteases have closely related homologs with nearly identical catalytic mechanisms, which often leads to cross-reactivity with inhibitors and unwanted side effects. Nevertheless, there have been many successful drugs that target proteases (Drag & Salvesen, 2010; Deu et al., 2012).

#### A Novel Drug Target in *S. aureus* and Related Bacteria

One way to combat the increasing prevalence of antibiotic resistant infections is to find novel antibiotic targets that require brand new classes of drugs. Our lab has recently discovered a novel drug target in *S. aureus* and related bacteria—the protease responsible for a newly discovered, essential N-terminal processing of ribosomal protein

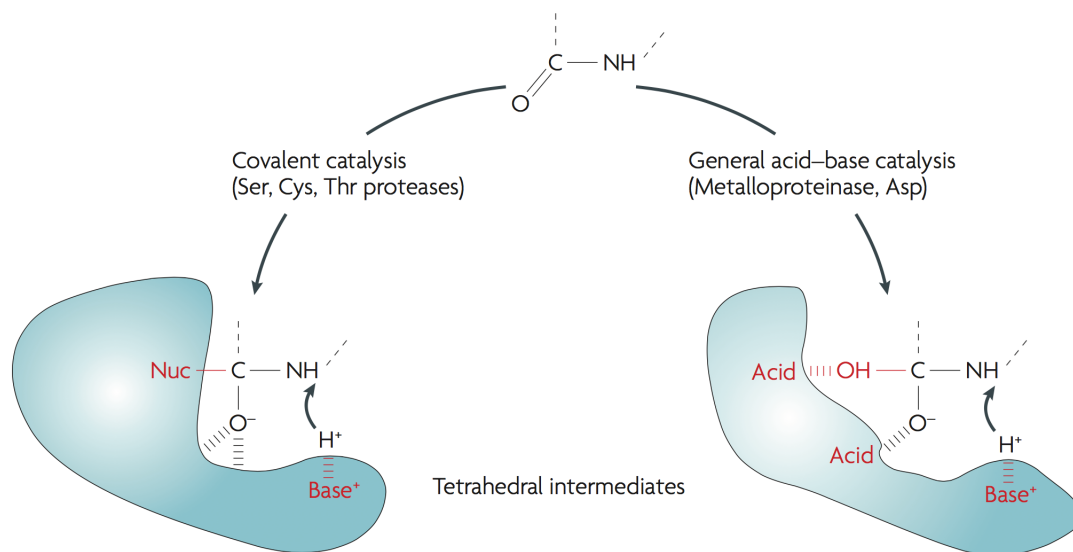


**Figure 1.3: Tetrahedral intermediates formed during peptide cleavage.**

A diagram of the tetrahedral intermediates formed during proteolysis. Serine (Ser), cysteine (Cys), and threonine (Thr) proteases form covalent bonds between the substrate and the enzyme's catalytic nucleophile (Nuc) during catalysis. Metalloproteases and aspartic acid proteases (Asp) use a non-covalent acid-base system involving a highly reactive water molecule.

Reprinted from *Nature Reviews: Drug Discovery*, 9, Drag, M., Salvesen, G.S., Emerging principles in protease-based drug discovery, 690-701, (2010), with permission from Nature Publishing Group.



L27. In *Escherichia coli*, the N-terminus of ribosomal protein L27 extends into the peptidyl transferase center and has been shown to contribute to 50S ribosomal subunit assembly, A- and P-site tRNA positioning and stability, and peptidyl transferase activity (Figure 1.4) (Lotti et al., 1987; Wower et al., 1998; Maguire et al., 2005; Voorhees et al., 2009; Shoji et al., 2011). Studies have shown that the first three N-terminal residues of *E. coli* L27—alanine 2, histidine 3, and lysine 4 (AHK)—are critical for facilitating translation (Maguire et al., 2005). However, in *S. aureus* and related bacteria, these critical residues (ASK) are located directly after an N-terminal extension of nine amino acids (Spilman et al., 2012). This N-terminal extension was discovered due to its homology to a cleavage motif in staphylococcal phage 80 $\alpha$  scaffold and major capsid proteins, which were found to be cleaved at their N-terminus at a conserved motif, KLKxNLQxF\*A (where \* denotes the cleavage site) (Poliakov et al., 2008). The homology between the N-termini of these proteins and the importance of the A(H/S)K motif for peptidyl transferase activity suggested that *S. aureus* L27 was also cleaved at this conserved motif and that this cleavage is required for proper ribosome function.

We confirmed this novel cleavage event in *S. aureus* and found that it is performed by a previously unclassified cysteine protease (Wall et al., 2015). This protease is encoded in an open reading frame (ORF) located between the genes for ribosomal proteins L21 (*rplU*) and L27 (*rpmA*) in *S. aureus* and related bacteria. All bacteria that encode the N-terminal extension of L27 have also been found to encode a homolog of this protease (Figure 1.5). The conservation of this N-terminal extension and the protease responsible for its cleavage in this subset of bacteria suggests that they

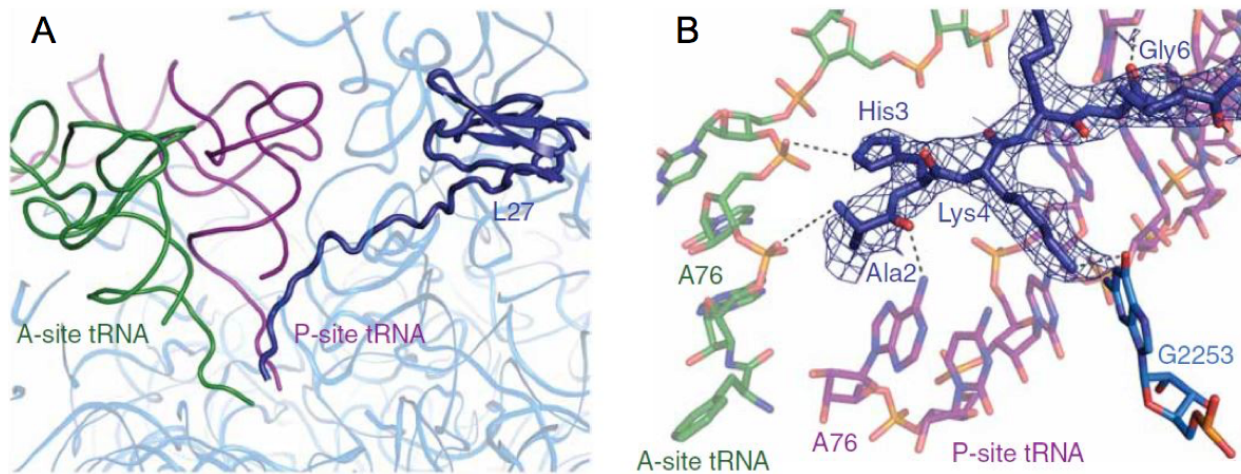


**Figure 1.4: Ribosomal protein L27 and tRNA at the PTC in *E. coli*.**

(A) A diagram of the N-terminus of ribosomal protein L27 (dark blue) in relation to the 3' ends of A- and P-site tRNAs (green and purple, respectively) at the PTC. (B) Predicted interactions of L27 with A- and P-site tRNAs and 23S RNA (light blue).

Reprinted/adapted from *Nature Structural and Molecular Biology*, 16 (5), Voorhees R.M., Weixlbaumer A., Loakes D., Kelley, A.C., Ramakrishnan V., Insights into substrate stabilization from snapshots of the peptidyl transferase center of the intact 70S ribosome, 528-533, (2009), with permission from Nature Publishing Group.

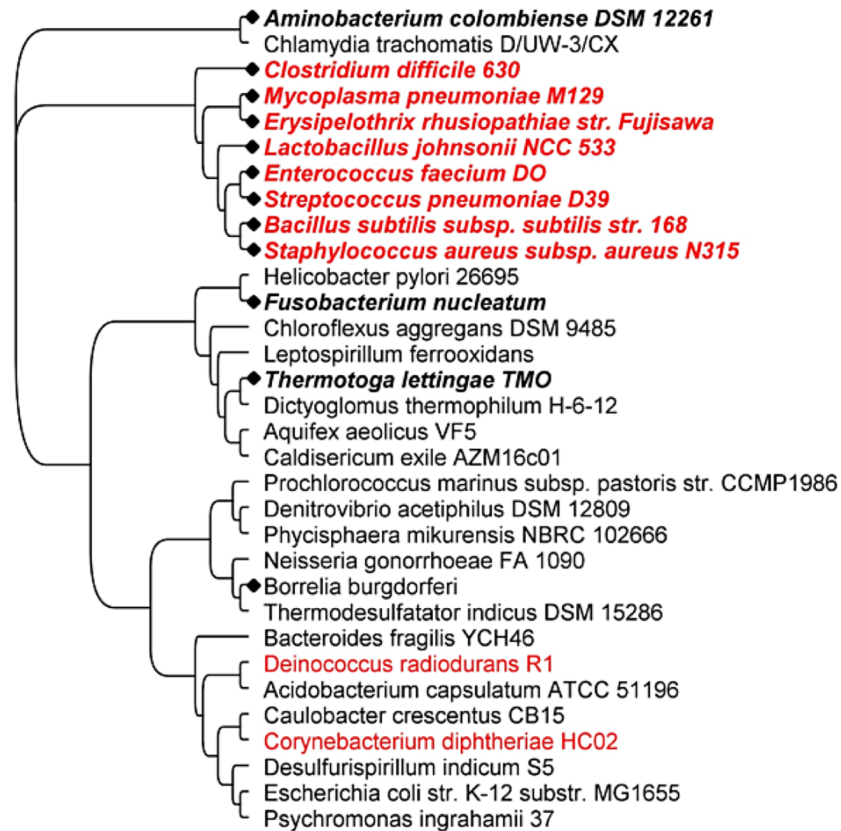


**Figure 1.5: L27 and Prp phylogeny across major bacterial phyla.**

A neighbor-joining phylogenetic tree (Jukes Cantor; BLOSUM80) consisting of sequences from representative species of each major bacterial phyla. Gram-positive species are designated in red. Gram-negative species are designated in black. Species containing the conserved N-terminal extension in L27 are bold and italicized. Species containing a Prp homolog are indicated by black diamonds.

Reprinted from *Molecular Microbiology*, 95 (2), Wall E.A., Caulfield J.H., Lyons, C.E., Manning K.A., Dokland, T., Christie, G.E., Specific N-terminal cleavage of ribosomal protein L27 in *Staphylococcus aureus* and related bacteria, 258-269, (2015), with permission from John Wiley and Sons.

play an important role in the biology of these organisms. We have named this newly discovered protease phage-related ribosomal protease, or Prp (Wall et al., 2015).

Both L27 and Prp have been shown to be essential in *S. aureus*. Therefore, cleavage of the N-terminal extension was thought to be an essential process as well. To test this, a complementation system was generated to determine if *S. aureus* could survive in the presence of pre-cleaved ( $\Delta 2-9$ ) or un-cleavable (F8A:F9A) variants of L27 (Figure 1.6). In this system, native *S. aureus* L27 was deleted from the chromosome and complemented with IPTG-inducible, wild-type L27 on a plasmid. This made *S. aureus* completely dependent on IPTG for survival. Then, a second, arsenite-inducible plasmid was introduced, which expressed wild-type, pre-cleaved, or un-cleavable L27. Using the different inducers, each of these L27 variants were expressed and their effects on cell survival were determined. In this system, only wild-type L27 could complement the chromosomal deletion, proving that its N-terminal cleavage is an essential process (Wall, 2015).

Due to its role in carrying out an essential and previously undescribed cleavage of L27, Prp is a promising target for novel antibiotics. The goal of this study was to characterize the activity and substrate specificity of Prp, which will provide insight into its function and lay the groundwork necessary for finding inhibitors of this enzyme. Towards this end, our lab has developed a fluorogenic peptide cleavage assay, based on the cleavage of a peptide 11-amino acids long, derived from the conserved cleavage motif of *S. aureus* ribosomal protein L27 (Figure 1.7). Flanking this peptide is a fluorophore, 2-aminobenzoic acid (2-abz), at its N-terminus and a quencher, dinitrophenol (Dnp), at its C-terminus. When Prp cleaves this substrate between the

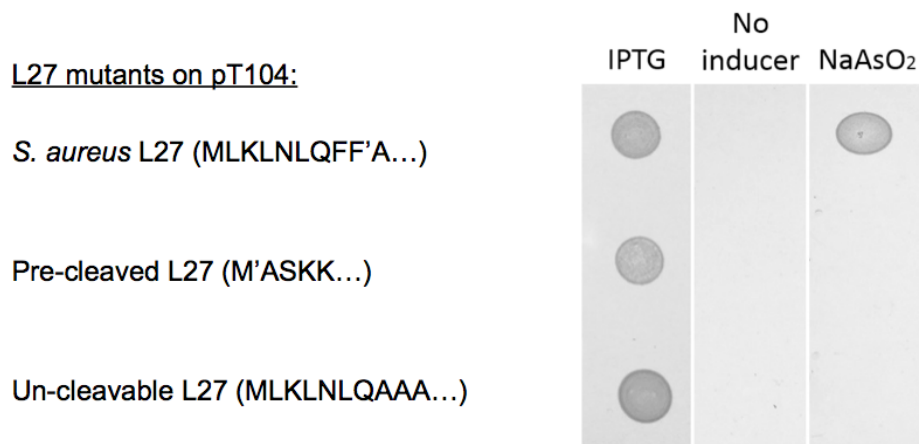
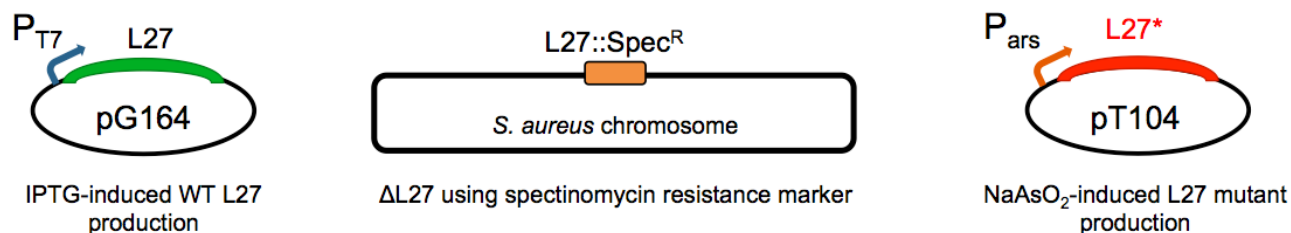


**Figure 1.6: An L27 complementation system.**

Native L27 was deleted from the *S. aureus* chromosome and replaced with a spectinomycin-resistance cassette (Spec<sup>R</sup>). An IPTG-inducible plasmid expressing wild-type L27 was introduced alongside an arsenite-inducible plasmid expressing wild-type, pre-cleaved, or un-cleavable L27 (L27\*). Results show that only wild-type L27 was able to complement the chromosomal deletion (Wall, 2015).

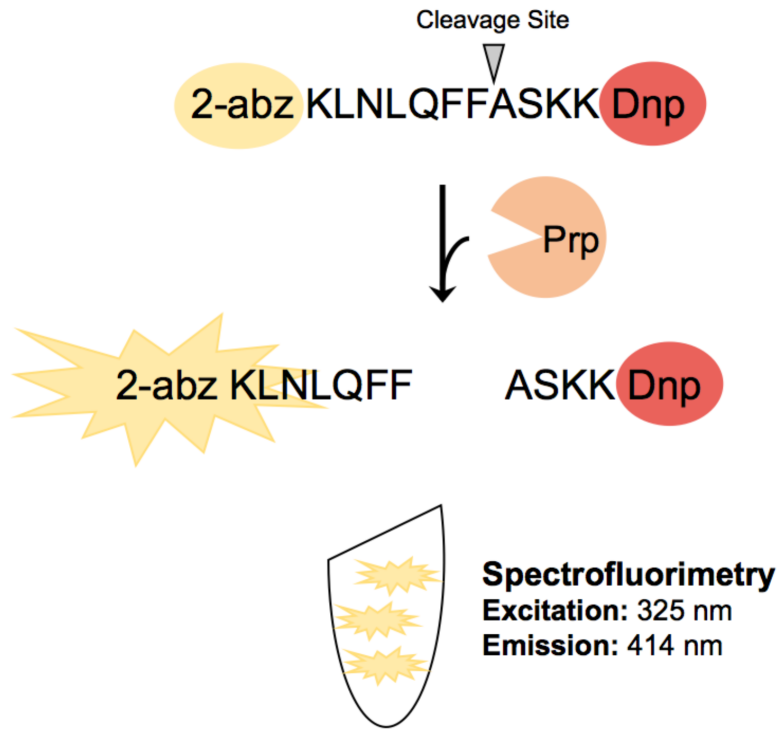


**Figure 1.7: Diagram of the fluorogenic peptide cleavage assay.**

In the assay used in this study, an 11-amino acid long peptide based on the conserved cleavage motif of *S. aureus* L27 is cleaved by Prp. Upon cleavage, the N-terminal fluorophore (2-abz) and C-terminal quencher (Dnp) are separated, causing an increase in fluorescence upon excitation at 325 nm. This increase in fluorescence is measured using a microplate reader (Adapted from Wall, 2015).

phenylalanine and alanine residues, the fluorophore and quencher are separated causing an increase in fluorescence intensity upon excitation at 325 nm. Using a Tecan Infinite<sup>®</sup> M1000 microplate reader, this assay was optimized and used to determine the enzyme kinetics of wild-type Prp, test its substrate specificity using competitive peptide substrates, and test predictions made based on a structural model using active-site mutants.

## **Chapter 2**

### **Materials and Methods**

Note: All reagents were procured through standard suppliers including Fisher Scientific (Waltham, MA) and Sigma-Aldrich (St. Louis, MO), unless otherwise specified.

#### **I. Bacterial Culture**

Bacterial strains used in this study are listed in Table 1. *E. coli* strains were cultured in Luria-Bertani (LB; Fisher Scientific; Waltham, MA) broth or on 1.5% LB agar plates supplemented with ampicillin (100 µg/ml) and/or chloramphenicol (30 µg/ml), as required, and grown at 37°C overnight. *S. aureus* strain RN4220 was cultured in LB broth or on 1.5% LB agar plates and incubated at 37°C overnight. Liquid cultures were grown on an orbital shaker at 200 rpm.

#### **II. DNA Manipulations**

Restriction endonucleases, restriction enzyme buffers, and bovine serum albumin (BSA) were purchased from New England Biolabs (Ipswich, MA) and used according to the manufacturer's instructions. Restriction digests were generally



**Table 1. Bacterial strains and plasmids used in this study**

<b><i>E. coli</i> strains</b>	<b>Description</b>	<b>Reference or source</b>
Stellar™ competent cells	HST08 derivative, high transformation efficiency strain. <i>E. coli</i> F <sup>-</sup> , <i>endA1</i> , <i>supE44</i> , <i>thi-1</i> , <i>recA1</i> , <i>relA1</i> , <i>gyrA96</i> , <i>phoA</i> , $\Phi$ 80d <i>lacZ</i> $\Delta$ M15, $\Delta$ ( <i>lacZYA-argF</i> )U169, $\Delta$ ( <i>mrr-hsdRMS-mcrBC</i> ), $\Delta$ <i>mcrA</i> , $\lambda$ <sup>-</sup>	Clontech
BL21-CodonPlus™ (DE3)-RIL competent cells	Stratagene BL21-Gold derivative. <i>E. coli</i> B F <sup>-</sup> <i>ompT</i> <i>hsdS</i> (r <sub>8</sub> <sup>-</sup> m <sub>8</sub> <sup>-</sup> ) <i>dcm</i> <sup>+</sup> Tet <sup>r</sup> <i>gal</i> $\lambda$ (DE3) <i>endA</i> Hte [ <i>argU</i> <i>ileY</i> <i>leuW</i> Cam <sup>r</sup> ]	Agilent Technologies
RN	Scarab cells containing pHYRS52 with His <sub>6</sub> -tagged ubiquitin-like protein-specific protease 1 (Ulp1) under control of T7/ <i>lac</i> promoter	Dr. Darrell Peterson
<b><i>S. aureus</i> strains</b>		
RN4220	Restriction-defective derivative of RN450	Kreiswirth, B.N., <i>et al.</i> , 1983.
<b>Plasmids for protein overexpression</b>		
pRW	pET21a derivative with T7/ <i>lac</i> promoter, Stu1 site, His <sub>6</sub> -SUMO tag, HindIII site, Xho1 site and T7 terminator	Dr. Darrell Peterson
pEW34	Plasmid pRW with His <sub>6</sub> -SUMO-tagged wild-type Prp	Wall, E. A.
pEW40	Plasmid pRW with His <sub>6</sub> -SUMO-Prp C34S (TGT → AGT)	Wall, E. A.
pALJ5	Plasmid pRW with His <sub>6</sub> -SUMO-Prp S38A (TCA → GCT)	This work
pALJ6	Plasmid pRW with His <sub>6</sub> -SUMO-Prp D31A (GAT → GCA)	This work
pALJ7	Plasmid pRW with His <sub>6</sub> -SUMO-Prp H22A (CAT → GCA)	This work
pALJ8	Plasmid pRW with His <sub>6</sub> -SUMO-Prp G21A (GGC → GCA)	This work

performed in 25  $\mu$ l reactions. Plasmid DNA was purified using the QIAprep<sup>®</sup> Spin Miniprep Kit (Qiagen; Valencia, CA) according to manufacturer's instructions. When applicable, plasmid DNA was eluted in HPLC-grade water for DNA sequencing. PCR products were analyzed and prepared for purification using agarose gel electrophoresis. The DNA bands were excised and the DNA was purified using a Nucleospin<sup>®</sup> Gel and PCR Clean-up Kit (Macherey-Nagel; Düren, Germany) according to manufacturer's instructions. The concentration of purified DNA was determined using a Nanodrop<sup>™</sup> 1000 spectrophotometer (Thermo Scientific; Waltham, MA). Cloning reactions were performed using an In-Fusion<sup>®</sup> HD Cloning Kit (Clontech Laboratories Inc.; Mountain View, CA) according to manufacturer's instructions.

### **III. Generating Prp Mutants**

#### **a. Isolation of Genomic DNA (Ligozzi and Fontana, 2003)**

To isolate the genomic DNA of *S. aureus*, 250  $\mu$ l of fresh RN4220 overnight culture was centrifuged at 14,000 rpm for five minutes to pellet the bacteria. The cells were resuspended in 100  $\mu$ l of EB buffer (Qiagen; Valencia, CA) and 2  $\mu$ l of lysostaphin (5 mg/ml) and incubated for 30 minutes in a 37°C water bath to lyse. Five hundred microliters of DNAzol<sup>™</sup> (Invitrogen; Grand Island, NY) was added, gently mixed by inversion, and the mixture was incubated for five minutes at 65°C. This mixture was then transferred to a QIAprep<sup>®</sup> Spin Miniprep column and centrifuged for one minute at 10,000 rpm to allow the gDNA to bind the column. The column was then washed with 750  $\mu$ l of PE buffer (Qiagen; Valencia, CA) and centrifuged for one minute at 10,000

rpm. The flow through was discarded and the column was spun again at 10,000 rpm for one minute to dry. The column was then washed with 750  $\mu$ l of 70% ethanol and centrifuged at 10,000 rpm for one minute and the flow through was discarded. The column was placed in a clean 1.5 ml microcentrifuge tube and 50  $\mu$ l of pre-warmed (65°C) EB buffer was added. After standing for five minutes at room temperature, the gDNA was eluted via centrifugation for one minute at 10,000 rpm. The gDNA from several isolations was concentrated using an Amicon<sup>®</sup> Ultra-0.5 Centrifugal Filter (EMD Millipore; Billerica, MA) according to manufacturer's instructions.

#### **b. Polymerase Chain Reaction (PCR)**

PCR reactions were performed using a T-Gradient Thermoblock thermocycler (Biometra; Göttingen, Germany). Primers used in this study are listed in Table 2 and were produced by Integrated DNA Technologies (Coralville, IA). Lyophilized primers were resuspended to 1 mM with HPLC-grade water and working primer stocks were made by 1:100 dilution with HPLC-grade water to 10  $\mu$ M. PCR amplification reactions were prepared as follows: 1X *PfuUltra* II reaction buffer (Agilent Technologies; Santa Clara, CA), 100  $\mu$ M dNTPs (Invitrogen; Grand Island, NY), DNA template (~10 ng of RN4220 gDNA), 0.2  $\mu$ M of each primer, and 0.5  $\mu$ l of *PfuUltra* II fusion HS DNA polymerase (Agilent Technologies; Santa Clara, CA) brought to a final reaction volume of 50  $\mu$ l with HPLC-grade water. PCR reaction master-mixes were made with 3.3X of each component and split into three 50  $\mu$ l reactions.

In general, the PCR thermocycling program was as follows: initial denaturation for 2 minutes at 95°C, followed by 32 cycles of denaturation for 20 seconds at 95°C,

**Table 2. Primers used in this study**

Primer	Sequence (5' → 3')	Purpose	Direction	T <sub>m</sub> (°C)	DNA Template
FIXEAW101	AGA ACA GAT TGG AGG* C ATG <u>ATT ACT GTT GAT ATT ACA GTT</u> AAT GAT GAA GG	Prp into pRW	F	55.6	RN4220
EAW102	GTG CGG CCG CAA GCT* TCA <u>CTT ATA ATT TAA TCT AAT ATT</u> CTC ATT ATA TTC TTC TTC AAT	Prp into pRW	R	55.2	RN4220
EAW185	GTC AGC (TGC) GCC ATC* CAT <u>AAT AAC GTC TGT TAC TTT G</u>	Prp H22A substitution	R	56.1	RN4220
EAW186	GAT GGC (GCA) <u>GCT GAC* CATG</u> GTG AAT ATG GTC	Prp H22A substitution	F	55.7	RN4220
EAW189	TAC AGC (AGC) AGC TCC* AGC <u>ACA AAC GAT ATC ATG ACC</u>	Prp S38A substitution	R	60.6	RN4220
EAW190	GGA GCT (GCT) GCT GTA* TTG <u>TTT GGT AGT GTT AAT GCG ATT</u> ATA GG	Prp S38A substitution	F	59.0	RN4220
EAW191	AAC GAT (TGC) ATG ACC* ATA <u>TTC ACC ATG GTC AGC ATG</u>	Prp D31A substitution	R	59.0	RN4220
EAW192	GGT CAT (GCA) <u>ATC GTT* TGT</u> GCT GGA GCT TCA GC	Prp D31A substitution	F	60.2	RN4220
EAW225	AGC ATG (TG)C ATC CAT* AAT <u>AAC GTC TGT TAC TTT GCC TTC</u>	Prp G21A substitution	R	57.6	RN4220
EAW226	ATG GAT G(CA) <u>CAT GCT* GAC</u> CAT GGT GAA TAT GGT C	Prp G21A substitution	F	57.9	RN4220
T7term	CTA GTT ATT GCT CAG CGG T	Sequencing Prp	R	52.0	pEW34, pEW40, pALJ5-8

Annealing sequence is underlined

T<sub>m</sub> corresponds to annealing sequence

Restriction sites marked with asterisks

Mutations in parentheses

primer annealing for 15 seconds, and primer extension for 15 seconds at 72°C. After these cycles was a final extension for three minutes at 72°C, then the reactions were chilled to 4°C or stored at -20°C. Annealing temperatures for each reaction were optimized based on the melting temperatures ( $T_m$ ) of the specific primers and were generally the average  $T_m-5^\circ\text{C}$ .

### **c. Agarose Gel Electrophoresis**

Analytical and preparatory gels were used to analyze whether PCR reactions were successful, to prepare PCR products for gel purification, or to verify the insertion of cloned genes into vectors. 1.3% and 2% agarose (KSE Scientific; Durham, NC) gels were cast in 1X Tris-acetate-EDTA (TAE) buffer with 0.3 µg/ml ethidium bromide.

Samples were prepared as follows (when applicable): one microliter of 6X loading dye (50% v/v glycerol, 50% v/v 1X TAE, tiny amount of bromophenol blue) was mixed with three microliters of HyperLadder™ IV (Bioline; Taunton, MA), 25 µl of 6X loading dye was added to ~150 µl of PCR product, 4 µl of 6X loading dye was mixed with 25 µl of restriction digested plasmid, and 1 µl of 6X loading dye was added to 1 µl of double-digested empty vector.

For analytical gels, 1.3% gels were used. Four microliters of HyperLadder™ IV mixture and 1 µl of PCR product sample were loaded onto the gel and electrophoresed in 1X TAE at 115 V for about one hour.

For preparatory gels, 1.3% gels were used. Four microliters of HyperLadder™ IV mixture and all of the remaining PCR product sample (~175 µl) were loaded onto the gel and electrophoresed in 1X TAE at 115 V for about one hour.

For verification of cloned genes inserted into vectors, 2% gels were used. Four microliters of HyperLadder™ IV mixture, the entire restriction digested plasmid sample, and 2 µl of double-digested empty vector were loaded onto the gel and electrophoresed in 1X TAE at 115 V for about one hour.

After electrophoresis, the gels were visualized using a White/UV transilluminator (VWR; Randor, PA) and photographed using a Fotodyne FOTO/Analyst® Apprentice - UV system (Heartland, WI) with a Canon PowerShot S100 (Melville, NY).

#### **d. Construction of Expression Plasmids**

Plasmids were constructed following the general scheme: preparation of the vector (bacterial culture, plasmid DNA extraction, restriction enzyme digestion, gel extraction), preparation of the gene of interest (bacterial culture, gDNA isolation and purification, PCR amplification, gel extraction), and In-Fusion® reaction to ligate the gene of interest into the vector. In-Fusion® reactions generally included ~60 ng of restriction enzyme-digested vector, ~20 ng of insert DNA, and 2 µl of 5X In-Fusion® HD Enzyme Premix brought to a final reaction volume of 10 µl with HPLC-grade water. The reactions were incubated for 15 minutes at 50°C then placed on ice. The reaction was then either used to transform competent cells or stored at -20°C. Vector control reactions were performed in the same manner but without the insert DNA.

#### **e. Bacterial Transformation**

To amplify and isolate newly generated plasmids, Stellar™ competent *E. coli* cells (Clontech Laboratories Inc.; Mountain View, CA) were transformed with the plasmids.

The cells were thawed on ice, then 50  $\mu$ l were pipetted into a 15 ml conical tube on ice along with 2.5  $\mu$ l of completed In-Fusion<sup>®</sup> reaction. The reaction was incubated on ice for 30 minutes, heat-shocked in a 42°C water bath for 45 seconds, then put back on ice immediately. After 1-2 minutes, 450  $\mu$ l of SOC medium (Clontech) was added to the reaction mixture and it was incubated on a 200 rpm orbital shaker at 37°C for one hour. After incubation, 5 and 100  $\mu$ l of the transformation reaction were plated on LB plates with the appropriate antibiotics. A concentrate was prepared by centrifuging the remaining reaction mixture in a 1.5 ml microcentrifuge tube for 3.5 minutes at 4000 rpm to pellet the bacteria. The supernatant was discarded and the cells were resuspended in the residual media by vortexing, then the remaining mixture was plated. The plates were incubated at 37°C overnight.

BL21-CodonPlus<sup>™</sup>(DE3)-RIL (Agilent Technologies; Santa Clara, CA) *E. coli* cells were used as the host strain for plasmids designed for protein overexpression. Competent cells were thawed on ice, then 100  $\mu$ l of cells were pipetted into a 15 ml conical tube on ice. Two microliters of 1:10 diluted XL10-Gold  $\beta$ -mercaptoethanol mix was added and the tube was swirled gently to mix. The cells were incubated on ice for 10 minutes, with gentle mixing every two minutes, then about 25 ng of plasmid DNA was added and the reaction was gently mixed. This reaction was incubated on ice for 30 minutes, then heat-pulsed<sup>™</sup> in a 42°C water bath for 20 seconds and placed back on ice for two minutes. Nine hundred microliters of prewarmed (42°C) SOC medium was added and the reaction was incubated on a 200 rpm orbital shaker at 37°C for one hour. After incubation, 5 and 100  $\mu$ l of the transformation reaction were plated on LB plates with the appropriate antibiotics. A concentrate was prepared by centrifuging the

remaining reaction mixture in a 1.5 ml microcentrifuge tube for 3.5 minutes at 4000 rpm to pellet the bacteria. The supernatant was discarded and the cells were resuspended in the residual media by vortexing, then the remaining mixture was plated. The plates were incubated at 37°C overnight.

To verify that genes of interest had been properly cloned, transformants were restreaked to isolate isogenic colonies and liquid cultures of candidates were prepared. The plasmids were purified by miniprep and digested using the same restriction enzymes that had initially been used to linearize the vector, then compared by agarose gel electrophoresis with the linear vector. If the insert was present, the plasmid was sent for sequencing by Eurofins MWG Operon (Huntsville, AL).

To freeze down and store the newly generated plasmids and autoexpression strains, liquid cultures were prepared, grown overnight, then mixed 1:1 with a 40% glycerol:LB solution, stored in labeled vials, and frozen at -80°C.

#### **IV. Expression and Purification of Recombinant Proteins**

##### **a. Recombinant Protein Overexpression via Autoinduction Culture**

Hexahistidine-small ubiquitin-related modifier (His<sub>6</sub>-SUMO) tagged Prp and His<sub>6</sub>-tagged ubiquitin-like protein-specific protease 1 (Ulp1) were overexpressed in BL21-CodonPlus™(DE3)-RIL and Scarab *E. coli* cells, respectively. The bacteria were grown in three one-liter cultures of autoinduction media containing 25 mM sodium phosphate (Na<sub>2</sub>HPO<sub>4</sub>; EMD Chemicals; Gibbstown, NJ), 25 mM potassium phosphate (KH<sub>2</sub>PO<sub>4</sub>), 50 mM ammonium chloride (MCB Reagents; Gibbstown, NJ), 5 mM sodium sulfate (EM



Science; Cherry Hill, NJ), 5 g/L yeast extract, and 10 g/L tryptone in deionized water. The media was autoclaved to sterilize and allowed to cool to room temperature. Each liter of media was then supplemented with 1X carbohydrate mixture (0.5% glycerol, 0.05% glucose, 0.2% lactose), 1 mM MgSO<sub>4</sub>, 100 µg/ml ampicillin (Ulp1 and Prp), 30 µg/ml chloramphenicol (Prp only), and 1 ml of fresh overnight culture and incubated overnight at 30°C on an orbital shaker at 200 rpm. The cultures were collected in one liter centrifuge bottles and pelleted in a Beckman Coulter Avanti® J-26 XP ultracentrifuge (Indianapolis, IN) for 15 minutes at 8,000 rpm at 4°C. The pellets were resuspended in approximately 100 ml of nickel column wash buffer (25 mM Tris, pH 8, 300 mM NaCl, 10 mM imidazole), collected in plastic bags, sealed with a heat sealer, and stored at -80°C until purification.

#### **b. Purification of Recombinant Proteins**

To purify the overexpressed His<sub>6</sub>-SUMO-Prp or His<sub>6</sub>-tagged Ulp1, bacterial pellets were thawed under running tap water, emptied into a beaker on ice, and stirred until evenly mixed. The bacteria were lysed using an Emulsiflex C3 High Pressure Homogenizer (Avestin Inc.; Ottawa, ON, CA) at ~20,000 psi and the lysate was collected in a clean beaker on ice. Fifty milliliter ultracentrifuge tubes were filled with lysate and weighed in pairs to balance, then the lysate was clarified by centrifugation at 20,000 rpm for 30 minutes at 10°C in an Avanti® J-27S XPI ultracentrifuge (Beckman Coulter; Indianapolis, IN). A nickel affinity column was prepared by adding 10-20 ml of Profinity™ IMAC Uncharged Resin (Bio-Rad; Hercules, CA), followed by 5-10 ml of 100 mM nickel sulfate (NiSO<sub>4</sub>). The column was washed with ~30 ml of wash buffer (25 mM

Tris, pH 8, 300 mM NaCl, 10 mM imidazole) and the clarified supernatant was added to the column, allowing the His<sub>6</sub>-tagged protein to bind the resin. The bound protein was washed and the absorbance of the flow-through was periodically read in a 1 cm pathlength quartz cuvette at 280 nm using a Bio-Rad<sup>®</sup> SmartSpec<sup>™</sup> 3000. Once the absorbance was  $\leq 0.050$  AU, the bound protein was eluted with ~100 ml elution buffer (25 mM Tris, pH 8, 300 mM NaCl, 110 mM imidazole) and ~3-5 ml fractions were collected. Once elution was complete, the absorbance of the fractions was measured to identify those containing protein. The fractions were then analyzed via SDS-PAGE alongside samples of the pellet, lysate, clarified supernatant, and nickel column wash flow-through. The fractions containing protein were pooled, sodium azide was added to 0.02% v/v, and the protein was dialyzed versus 50 mM sodium phosphate buffer, pH 7.5 with 0.02% v/v sodium azide (and 10% v/v glycerol for Ulp1).

### **c. Cleavage of the His<sub>6</sub>-SUMO Tag from Prp**

To cleave the His<sub>6</sub>-SUMO tag from purified and dialyzed His<sub>6</sub>-SUMO-Prp, His<sub>6</sub>-tagged Ulp1 was added in a ~1:1 by weight ratio with His<sub>6</sub>-SUMO-Prp with 150 mM NaCl. The reaction was agitated by hand at room temperature intermittently for about four hours. Five microliter samples were taken at t=0h, 1h, 2h, and 3h and analyzed for extent of cleavage via SDS-PAGE. After sufficient cleavage, the reaction was centrifuged for 10 minutes at 20,000 rpm at 10°C and purified via nickel affinity chromatography in the same manner as the tagged protein, except fraction collection began immediately after the sample was applied to the column. After dialyzing, the purified, tagless protein in solution was filter sterilized using a Millex<sup>®</sup> 0.22  $\mu$ m syringe

filter (EMD Millipore; Billerica, MA), a 40% v/v glycerol stock was made, and it was stored in one milliliter aliquots at -20°C.

#### **d. Sodium Dodecyl Sulfate-Polyacrylamide Gel Electrophoresis (SDS-PAGE)**

Proteins were analyzed via SDS-PAGE using a Bio-Rad® Mini PROTEAN® system (Hercules, CA). Gels were cast with a 12.5% resolving gel (187.5 mM Tris, 1.7 mM SDS, pH 8.8) and 10% stacking gel (250 mM Tris, 70 mM SDS, pH 6.8). Samples were prepared as follows: five microliters of the pellet, lysate, clarified supernatant, and flow-through were each mixed with 20 µl of deionized water and 25 µl of 2X sample buffer (100 mM Tris, pH 6.8, 4% w/v SDS, 20% v/v glycerol, 0.1% w/v bromophenol blue, 10% v/v β-mercaptoethanol) and 25 µl of each eluted fraction was mixed with 25 µl 2X sample buffer. The samples were boiled for two minutes then 10 µl of each prepared sample was loaded onto the gel and electrophoresed at a constant current of 30 mA for 50 minutes using a Bio-Rad® Mini-PROTEAN® Tetra Cell with a Bio-Rad® PowerPac™ Basic power supply. Running buffer was composed of 45 mM Tris, 382 mM glycine, and 3.5 mM SDS. After running the gel, it was stained (50% v/v methanol, 10% v/v acetic acid, 40% v/v deionized water, 0.2 % w/v coomassie brilliant blue R250) for 15 minutes then destained (10% v/v acetic acid, 30% v/v methanol, 60% v/v deionized water) overnight. The gel was visualized using a custom light-box and photographed using ArcSoft WebCam Companion® software with an HP® Webcam HD-2200.

#### **e. Bradford Protein Quantification Assay (Kruger, 2009)**

To determine the concentration of purified Prp, a Bradford protein quantification assay was used. Bradford reagent was made by first dissolving 10 mg of Coomassie blue G250 (BioRad; Hercules, CA) in 5 ml of 95% ethanol. Ten milliliters of 85% phosphoric acid was added and this solution was brought to 100 ml with deionized water. It was then gravity filtered through Whatman<sup>®</sup> No. 1 filter paper and stored in an amber bottle at room temperature. To prepare the protein standards, 1 mg/ml BSA was diluted with 50 mM sodium phosphate buffer (pH 7.5) to 0.1 mg/ml. This stock was then used to make a series of 100  $\mu$ l standards with concentrations of 0.1, 0.08, 0.06, 0.04, 0.02, and 0.01 mg/ml BSA with a 0 mg/ml BSA (100  $\mu$ l of 50 mM sodium phosphate buffer, pH7.5) blank. One hundred microliter purified Prp protein samples were prepared via dilution with buffer for 1:10, 1:20, and 1:100 samples. One milliliter of Bradford reagent was then added to each of the standards and samples and gently mixed. Two hundred and ten microliters of the blank, standards, and samples were pipetted in duplicate into a clear, flat-bottomed, 96-well plate (Greiner Bio-One; Monroe, NC) and assayed at 595 nm using a SpectraMax<sup>®</sup> 250 microplate reader with the Bradford protein quantitation template in the SoftMax<sup>®</sup> Pro data analysis software (Molecular Devices; Sunnyvale, CA). The results were printed, saved, and used to calculate the concentration of the undilute Prp sample.

## **V. Fast Protein Liquid Chromatography (FPLC)**

Fast protein liquid chromatography was performed on a sample of tagless, wild-type Prp with His<sub>6</sub>-tagged Ulp1 present using an ÄKTA<sub>FPLC</sub><sup>™</sup> system with UNICORN<sup>™</sup> system control software and a 125 ml P-10<sup>™</sup> size-exclusion column (20,000 MWCO; Bio-Rad; Hercules, CA) equilibrated to 50 mM sodium phosphate buffer, pH 7.5. Five milliliters of Prp:Ulp1 sample was manually injected onto the column and eluted with 50 mM sodium phosphate buffer, pH 7.5. Two-milliliter fractions were collected at a flow rate of 1 ml/min while the elution profile was monitored spectrophotometrically at 280 nm. Peak fractions were analyzed via SDS-PAGE.

## **VI. Fluorogenic Peptide Cleavage Assay, Generating a Standard Curve and Determining the Extent of Assay Completion, and Data Analysis**

### **a. Fluorogenic Peptide Cleavage Assay**

Peptides used in this study were purchased from United Biosystems (Herndon, VA) and are listed in Table 3. Stock fluorogenic peptide (SauL2711) was made by dissolving a small amount of lyophilized peptide in DMSO. Its concentration was determined by measuring its absorbance in a 0.1 cm pathlength quartz cuvette at 325 nm with a Bio-Rad<sup>®</sup> SmartSpec<sup>™</sup> 3000 and dividing this number by its molar extinction coefficient (2,850 L cm<sup>-1</sup> mol<sup>-1</sup>). Aliquots were frozen at -20°C until use.

Competitive peptides used in this study were resuspended to 10 mM with DMSO. One millimolar working stocks were stored at -20°C until use.

**Table 3. Synthetic peptides used in this study**

<b>Peptide</b>	<b>Sequence</b>	<b>Length (# of AAs)</b>	<b>Description</b>
SauL2711	2-Abz- <b>KLNLQFF*ASKK</b> (Dnp)	11	Fluorogenic peptide based on L27 cleavage sequence
EW11	Ac- <b>KLNLQFF*ASKK</b> -NH <sub>2</sub>	11	Peptide based on L27 cleavage sequence
EW10	Ac- <b>LNLQFF*ASKK</b> -NH <sub>2</sub>	10	Peptide based on L27 cleavage sequence
EW8	Ac- <b>NLQFF*ASK</b> -NH <sub>2</sub>	8	Peptide based on L27 cleavage sequence
EW6	Ac- <b>QFF*ASK</b> -NH <sub>2</sub>	6	Peptide based on L27 cleavage sequence
CP13	Ac- <b>KLKLNLQHF*ASNN</b> -NH <sub>2</sub>	13	Peptide based on 80 $\alpha$ capsid cleavage sequence
CP11	Ac- <b>KLNLQHF*ASNN</b> -NH <sub>2</sub>	11	Peptide based on 80 $\alpha$ capsid cleavage sequence

\* denotes site of cleavage

Cleavage assays were performed using a Tecan Infinite<sup>®</sup> M1000 microplate reader with Magellan<sup>™</sup> data analysis software (Männedorf, Switzerland) and Greiner<sup>®</sup> Bio-One black, flat-bottomed, chimney well, non-sterile, non-binding, 96-well microplates (Monroe, NC).

Assays were standardized with respect to pH and concentration of dithiothreitol (DTT), ethylenediaminetetraacetic acid (EDTA), and sodium chloride (NaCl). Standardized assays had final concentrations of 1.5 mM DTT, 2.35 mM EDTA, 2.53% DMSO, and various concentrations of fluorogenic peptide and/or competitive peptide in 50 mM sodium phosphate buffer, pH 7.0. Two milliliters of each assay sample were prepared (1 blank, 4 trials) and 190  $\mu$ l was pipetted into wells containing 10  $\mu$ l of 0.01 mg/ml Prp (21.38 nM final concentration) or 10  $\mu$ l of no-enzyme blank (40% glycerol, 0.02% sodium azide, sodium phosphate buffer, pH 7.5) for final assay volumes of 200  $\mu$ l.

The plate reader was set to read fluorescence intensity at an excitation wavelength of 325 nm and an emission wavelength of 414 nm with 5 nm bandwidths. Cleavage reactions were read at 8-second intervals for 10 minutes at ambient temperature. The plate reader's gain was optimized at 255 and the Z-position height was optimized at 20,450  $\mu$ m. The Magellan<sup>™</sup> assay protocol was saved as Abz\_Dnp\_ALJ Data were exported to Microsoft<sup>®</sup> Excel<sup>®</sup> (Redmond, WA) and saved for further analysis.

## **b. Generating a Standard Curve and Determining the Extent of Assay Completion**

To convert the raw values of relative fluorescence units (RFU) versus time from the assay data to concentration of fluorogenic substrate cleaved versus time, a standard curve of RFU versus concentration of fluorogenic substrate cleaved was prepared (Figure 2.1). Ten microliters of 1 mg/ml trypsin resuspended in 50 mM sodium phosphate buffer, pH 7.5, with 40% glycerol and 0.02% sodium azide was used in the standard cleavage assay with varying amounts of substrate (0-1.0  $\mu$ M). A no-enzyme blank was used to correct for background. The blank-corrected RFU values from four completed reactions at each concentration were averaged and the results were plotted versus the concentration of substrate included in the reaction.

Trypsin was also used in assays to determine the extent of assay completion by Prp. Identical assays were performed, cleaving 2  $\mu$ M substrate with 10  $\mu$ l of 1 mg/ml trypsin and Prp and the average absolute RFU values for four completed reactions were compared. Results indicated that both reactions approached the same RFU values, indicating that both reactions proceeded to the same extent of completion (Figure 2.2).

## **c. Data Analysis**

Assay data were analyzed using Microsoft<sup>®</sup> Excel<sup>®</sup> 2011 and GraphPad Prism<sup>®</sup> (La Jolla, CA). Data were collected and organized in Excel<sup>®</sup>, then the blank RFU value at each timepoint was subtracted from the corresponding timepoint of each trial for each assay. The blank-corrected RFU data were then converted to concentration of substrate cleaved using the equation of the standard curve (Figure 2.1) and plotted using a



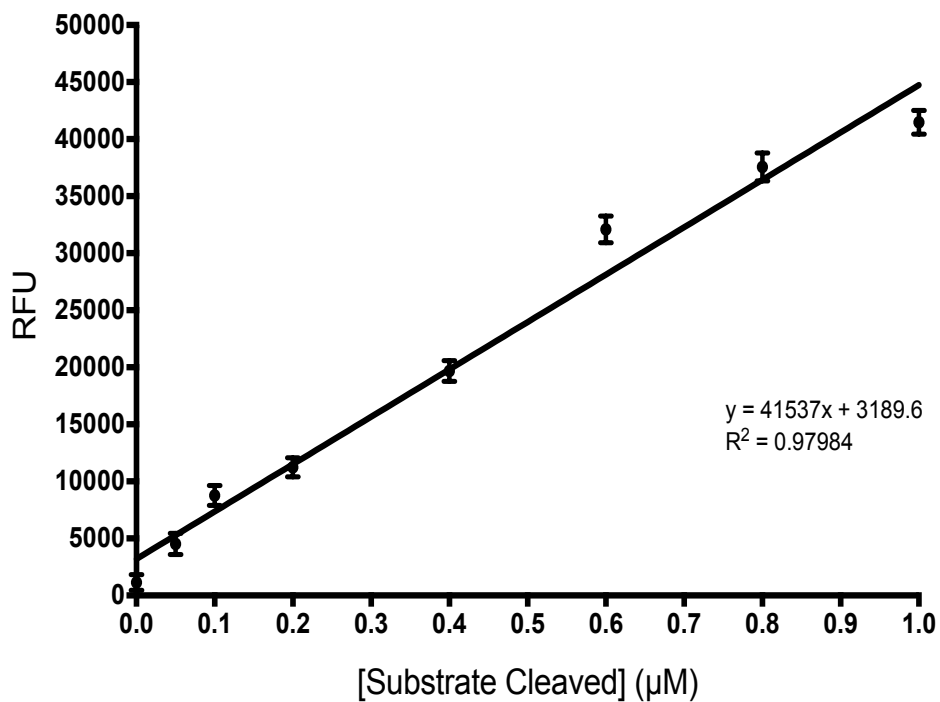


**Figure 2.1. Standard curve for converting raw RFU values from Prp assays to concentration of fluorogenic substrate cleaved.**

A standard curve generated by cleaving varying amounts of fluorogenic peptide using trypsin. The equation of the standard curve was used to convert the raw RFU values from Prp assays to concentrations of substrate cleaved.

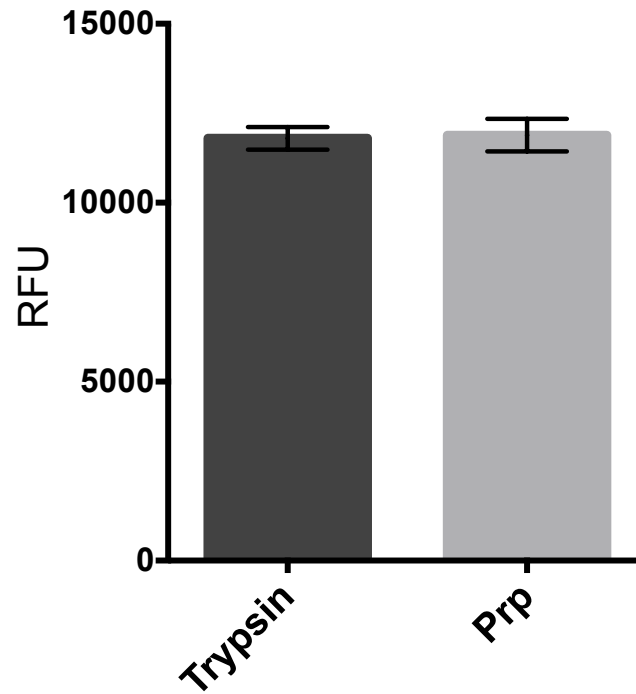


**Figure 2.2. Comparing absolute RFU values between completed reactions with trypsin and Prp.**

Two micromolar fluorogenic substrate was cleaved with the same amount of trypsin and Prp. The absolute RFU values from four completed reactions were averaged and indicated that both reactions proceeded to the same extent of completion.

smooth marked scatter plot. The slope of the initial, linear portion of each curve (initial velocity) was determined for each assay.

For enzyme kinetics data for the wild-type enzyme, the initial velocities for each substrate concentration were entered into Prism<sup>®</sup>, where the data were analyzed using non-linear regression fits to the Michaelis-Menten kinetics and  $k_{cat}$  equations ( $E_T$  constrained to 42.765 nM active sites).

For competition data from assays with competitive-peptide inhibitors, the percent activity and percent inhibition relative to a no-inhibitor control were calculated from the initial velocities for each inhibitor assay. These results were then entered into Prism<sup>®</sup> and analyzed using an ordinary one-way ANOVA, comparing the mean initial velocity for each inhibitor to that of the no-inhibitor control.

For activity data for the Prp active-site mutants, the percent activity relative to a wild-type control was calculated from the initial velocities for each mutant assay. These results were then entered into Prism<sup>®</sup> and analyzed using an ordinary one-way ANOVA, comparing the mean initial velocity for each mutant to that of the wild-type enzyme.

## Chapter 3

### Expression and Purification of Wild-type Prp and Generation of Active-site Mutants

Expression and purification of wild-type Prp were the first steps toward its biochemical characterization. The gene for wild-type Prp had been previously cloned by our lab into the T7 overexpression vector pRW, generating His<sub>6</sub>-SUMO-tagged Prp. This vector places the expression of the fusion protein under the control of the *T7lac* promoter, which contains a copy of the *lacO* operator sequence downstream of the T7 promoter. A plasmid-encoded copy of the LacI<sup>q</sup> repressor tightly binds this operator sequence and prevents basal transcription of the target gene in the absence of induction (Studier & Moffatt, 1986; Dubendorff & Studier, 1991).

BL21-CodonPlus<sup>™</sup> (DE3)-RIL competent cells, which contain a chromosomal copy of the T7 RNA polymerase under the control of the *lacUV5* promoter, were transformed with the expression plasmid. This promoter has mutations that remove the need for CRP:cAMP:promoter complex formation, allowing high-level expression of the T7 RNA polymerase upon induction (Pribnow, 1975; Sweet, 2003; Studier, 2005).

To induce protein expression, cells transformed with the expression plasmid were grown in autoinduction media, which is supplemented with 0.5% glycerol, 0.05% glucose, and 0.2% lactose. In this method of induction, glucose acts as the primary

carbon source during bacterial growth and is utilized first, which also suppresses basal target protein expression. As the cells run out of glucose and begin to ferment lactose, the *lacUV5* and *T7lac* promoters are derepressed, inducing expression of the T7 RNA polymerase, which subsequently transcribes the gene for the target protein. The presence of glycerol in the media provides a carbon source for sustained cell growth after induction. This method of induction generally yields higher quantities of protein and is easier to accomplish than the usual route of IPTG induction (Studier, 2005).

After expression of the fusion protein, the next steps were its purification and removal of the His<sub>6</sub>-SUMO tag. This tag can be efficiently cleaved by the protease Ulp1 at a Gly-Gly motif found at the C-terminus of the SUMO moiety (Malakhov et al., 2004). After an initial purification of His<sub>6</sub>-SUMO-tagged Prp by nickel affinity chromatography, His<sub>6</sub>-tagged Ulp1 was used to cleave away the His<sub>6</sub>-SUMO tag, leaving unmodified Prp. In determining the best route for the purification of tagless Prp, a sample of post-cleavage Prp with His<sub>6</sub>-tagged Ulp1 present was run on FPLC on a P10 size-exclusion column (MWCO=20,000). Our hope was that tagless Prp (MW=11,691.79) would elute from the column first, leaving His<sub>6</sub>-tagged Ulp1 (MW=27,394.05) behind. However, the elution profile from this column only showed one peak and subsequent SDS-PAGE analysis of the protein-containing fractions showed that tagless Prp and His<sub>6</sub>-tagged Ulp1 had co-eluted (Figure 3.1). These results, and previous structural studies (Chirgadze et al., 2014), indicated that Prp was a dimer with an approximate molecular weight of 23,383. Due to this complication, adjustments had to be made to the purification scheme. The nickel affinity-purified His<sub>6</sub>-SUMO-Prp was dialyzed to remove the elution buffer, which would prevent the hexahistidine tag from re-binding to the

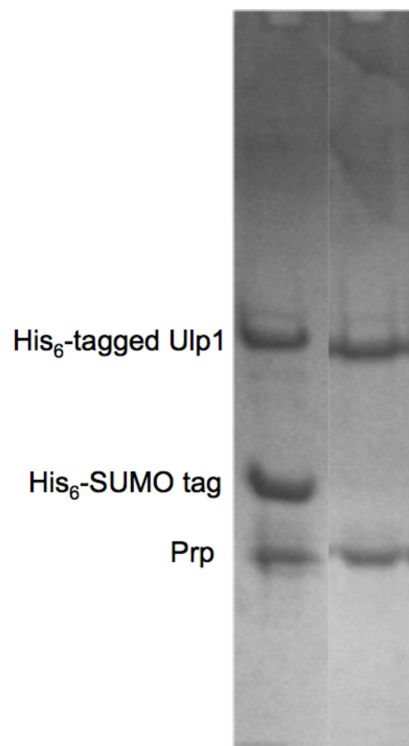


**Figure 3.1: SDS-PAGE gel of His<sub>6</sub>-tagged Ulp1 and Prp from P10 column.**

The left lane of this composite gel shows cleaved His<sub>6</sub>-SUMO Prp with His<sub>6</sub>-tagged Ulp1 present before size-exclusion FPLC. The right lane shows a sample from the FPLC fraction with the highest peak, showing that His<sub>6</sub>-tagged Ulp1 and tagless Prp co-eluted.

nickel affinity column. His<sub>6</sub>-tagged Ulp1 was again used to cleave away the His<sub>6</sub>-SUMO tag and the tagless protein was purified via nickel affinity chromatography. Through this route, tagless Prp was eluted directly from the column while the His<sub>6</sub>-SUMO tag and His<sub>6</sub>-tagged Ulp1 remained bound (Figure 3.2).

The fractions containing purified Prp were pooled and dialyzed and the concentration of protein was determined using a Bradford assay (Kruger, 2009). The concentration of protein in the pooled fractions was determined to be approximately 1.7 mg/ml. For long-term storage, a 40% glycerol:0.02% sodium azide freezer stock was made and the protein was stored at -20°C until characterization. The final concentration of the freezer stock was approximately 1.0 mg/ml.

In addition to the wild-type protein, several active-site mutants were generated in order to determine the effects of the mutations on catalysis and substrate binding and test predictions made based upon a structural model. Mutations in *prp* were introduced during PCR amplification using overlapping internal forward and reverse primers containing the desired codon changes (Table 2). Here, the target gene was amplified in two separate fragments, which were ligated together along with the vector during the In-Fusion<sup>®</sup> cloning reaction. Successful reactions were confirmed by Sanger sequencing.

Mutations were introduced at residues previously shown to be highly conserved near the active site or in the catalytic residues themselves (Wall et al., 2015). These residues include the catalytic cysteine (C34; Wall et al., 2015), the catalytic histidine (H22), a highly conserved serine (S38), and completely conserved glycine and aspartic acid residues (G21 and D31) (Figure 3.3). Each of these residues was changed to alanine except for the catalytic cysteine, which was replaced with a serine.

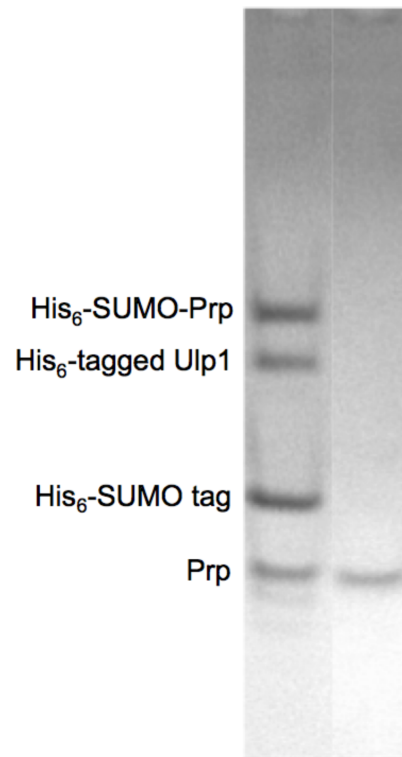


**Figure 3.2: SDS-PAGE gel of Prp pre- and post-purification.**

The left lane of this composite gel shows the His<sub>6</sub>-SUMO-Prp:His<sub>6</sub>-tagged Ulp1 cleavage reaction before purification by nickel affinity chromatography. The right lane shows purified, tagless Prp that was eluted during the second nickel affinity chromatography purification step.



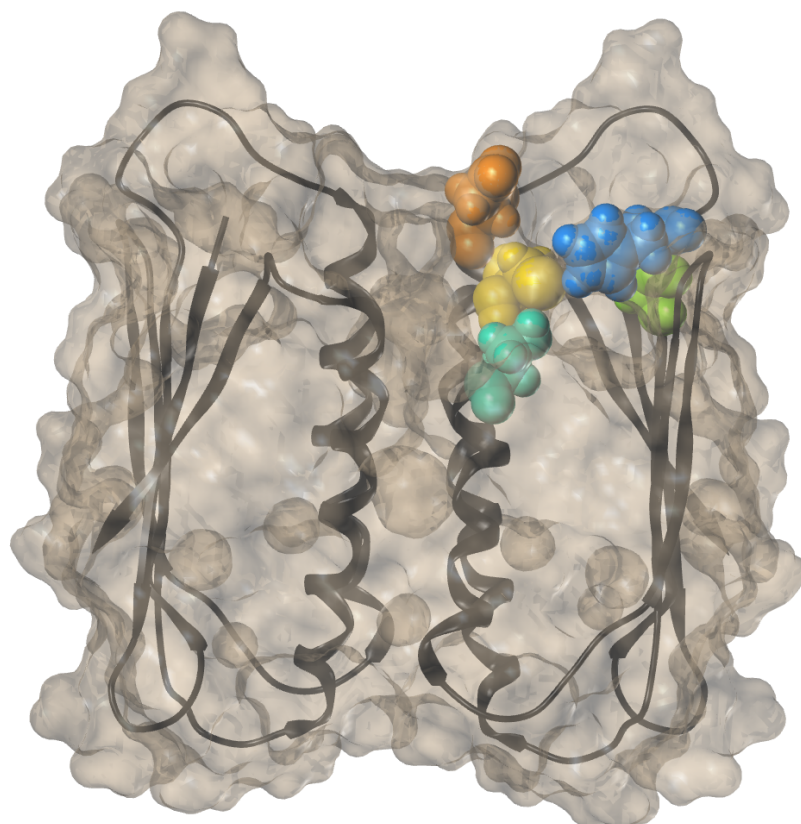


**Figure 3.3: Active-site mutations introduced into Prp.**

A molecular model of the Prp dimer showing a ribbon model under a transparent surface model. The active-site residues changed in this study are shown as space-filling atoms. The teal residue is S38, orange is D31, blue is H22, green is G21, and yellow is C34. The model was made in SYBYL based on a previous crystal structure of Prp (PDB ID: 2p92) [Created by Dr. Erin A. Wall].

These residues were replaced with alanine because it effectively removes side chain function while preserving the protein's backbone structure, which can provide clues to the function of the side chains in the wild-type protein (Peracchi, 2001). Serine was chosen because it is the same size as cysteine, with a hydroxyl group replacing the nucleophilic thiol, which has previously been shown to inactivate Prp (Wall et al., 2015). This result also indicates that replacing the catalytic cysteine with serine does not allow Prp to function as a serine protease. Each of these mutants was expressed, purified, and stored in the same manner as the wild-type protein until their characterization.

## Chapter 4

### Standardization of a Fluorogenic Peptide Cleavage Assay

To characterize the activity and substrate specificity of wild-type Prp and determine the effects of active-site mutations on substrate binding and catalysis, we have developed a fluorogenic peptide cleavage assay (Figure 1.7). Before beginning characterization, the optimum settings for the plate reader were determined based on several test assays. Various volumes of Prp were mixed with various concentrations of fluorogenic substrate and the run time, number of reads, temperature, z-position (position of the microplate versus the measuring head), and gain (sensitivity of the photomultiplier tube) were optimized. Based on these tests, assays were read at ambient temperature for 10 minutes with 8 second reads; the z-position for all assays was set to 20,450  $\mu\text{m}$ ; and the gain was set to 255 (unless otherwise noted). After determining the optimum settings for the plate reader, the conditions for the assay were optimized with respect to pH and concentration of DTT, EDTA, and sodium chloride.

Enzymatic activity can be greatly affected by pH; therefore, it was necessary to find a suitable buffer system and pH where Prp showed the highest activity. To optimize the pH of the assay, 50 mM sodium phosphate buffer was prepared at various pHs (5.5, 6.0, 6.5, 7.0, 7.5, and 8.0) and assays were performed in each of these buffers. Fluorogenic substrate was added to each of the buffers (35  $\mu\text{M}$  final concentration) and

they were mixed with one microliter of 1.0 mg/ml Prp (213.8 nM final concentration) and the increase in fluorescence intensity was measured. Initial velocities from three trials at each pH were averaged and indicated an optimum activity at pH 7.0 (Figure 4.1). This pH was used for all future assays.

Dithiothreitol is a reagent commonly used to reduce and prevent formation of disulfide bonds in proteins. Prp is a cysteine protease that has two solvent-exposed cysteine residues per molecule; therefore, the addition of DTT in the assay may prevent intermolecular disulfide bond formation, which could potentially lead to inactivation of the enzyme. Various concentrations of DTT were added to 50 mM sodium phosphate buffer, pH 7.0, along with 35  $\mu$ M fluorogenic substrate. Assays were performed identically to those for pH and the initial velocities from four trials were averaged. The results indicated no significant difference in activity over the range tested (Figure 4.2). We chose a concentration of 1.5 mM DTT to use in further assays.

Ethylenediaminetetraacetic acid is a chelating agent that sequesters metal ions in solution. Some enzymes use metal ions as cofactors (such as metalloproteases) and will not function in their absence (Bisswanger, 2014). If Prp requires metal ions to function, their sequestration would cause a decrease in activity. To test the dependence of Prp activity on the presence or absence of metal ions, the concentration of EDTA was varied in the assay in the same manner as DTT and the initial velocities from four trials were averaged. Results indicated highest activity at around 2.4 mM and above (Figure 4.3). A concentration of 2.35 mM EDTA was used in further assays.

Sodium chloride can affect the ionic strength of a solution, which is an important factor to consider in enzymatic assays. Very high or very low ionic strength can affect

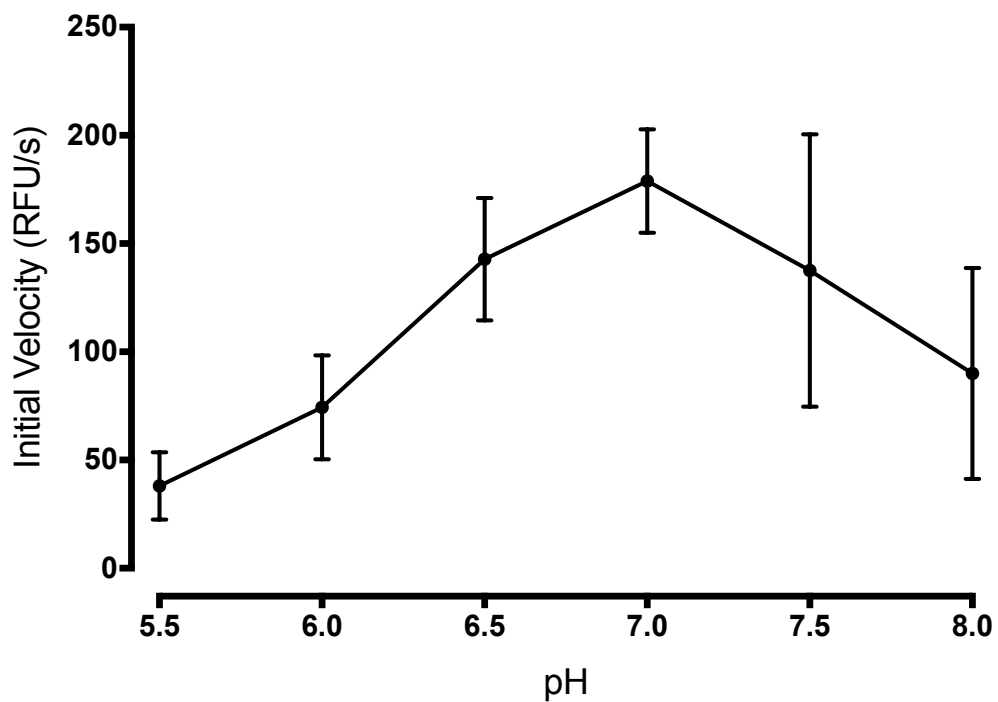


**Figure 4.1: Effect of pH.**

Assays were performed in sodium phosphate buffers with varying pH. The initial velocity of each reaction was determined and plotted versus pH. The highest initial velocity was observed at pH 7.0.

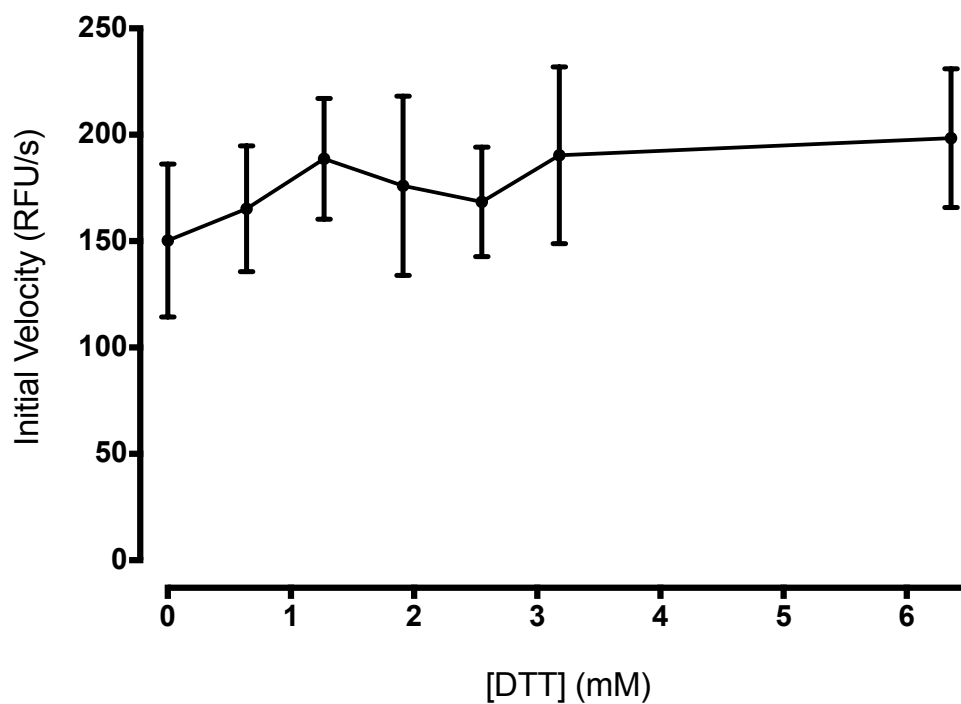


**Figure 4.2: Effect of DTT.**

Assays were performed with various amounts of added DTT. The initial velocity of each reaction was determined and plotted versus the concentration of DTT in the reaction. No significant difference in activity was seen over the range tested. 1.5 mM DTT was used in further assays.

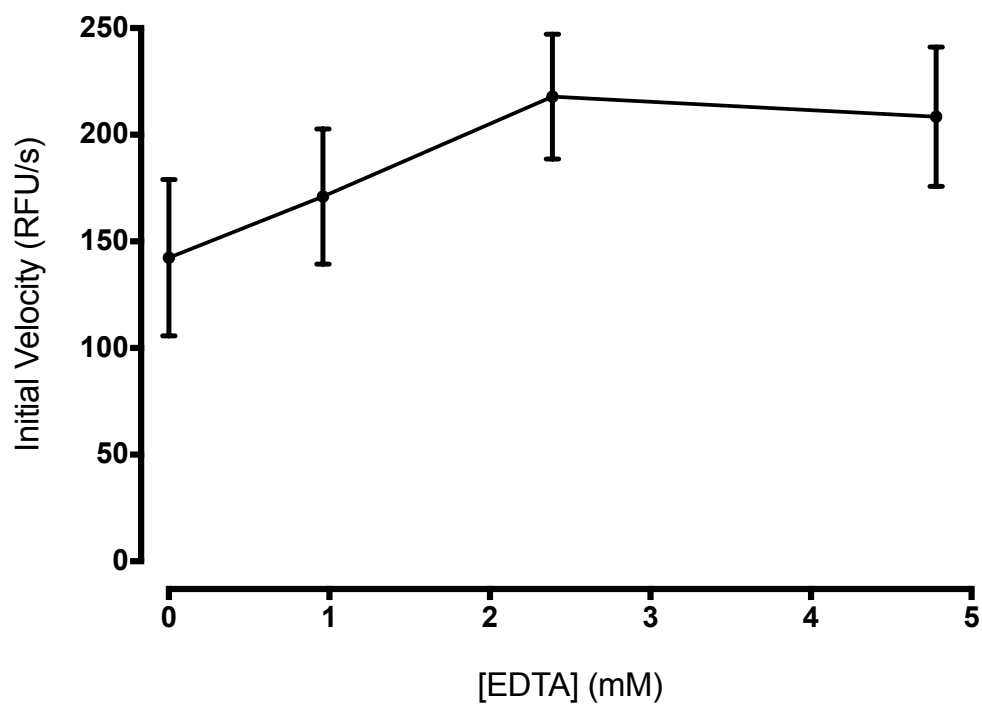


**Figure 4.3: Effect of EDTA.**

Assays were performed with various amounts of added EDTA. The initial velocity of each reaction was determined and plotted versus the concentration of EDTA in the reaction. The highest initial velocity was observed around 2.4 mM EDTA and above.

the activity of an enzyme or destabilize protein structure (Bisswanger, 2014). The concentration of sodium chloride in the assay was varied and the averaged initial velocities from four trials indicated that the assays with no sodium chloride gave the highest activity, with decreasing activity at higher concentrations (Figure 4.4). Therefore, it was excluded from further optimizations.

After testing the effects of these substances and conditions separately, the concentrations of each that gave highest initial velocity were combined to determine if they had an additive effect. Fifty millimolar sodium phosphate buffer, pH 7.0, alone; 1.5 mM DTT alone; and 2.35 mM EDTA alone were tested alongside 50 mM sodium phosphate buffer, pH 7.0, with 1.5 mM DTT and 2.35 mM EDTA. Averaged initial velocities from four trials showed that the combination of sodium phosphate buffer, DTT, and EDTA gave a slightly higher average initial velocity than either DTT or EDTA alone, although this difference was not statistically significant (Figure 4.5). Based on these results, the conditions for all future assays were standardized to 50 mM sodium phosphate buffer, pH 7.0, with 1.5 mM DTT and 2.35 mM EDTA.



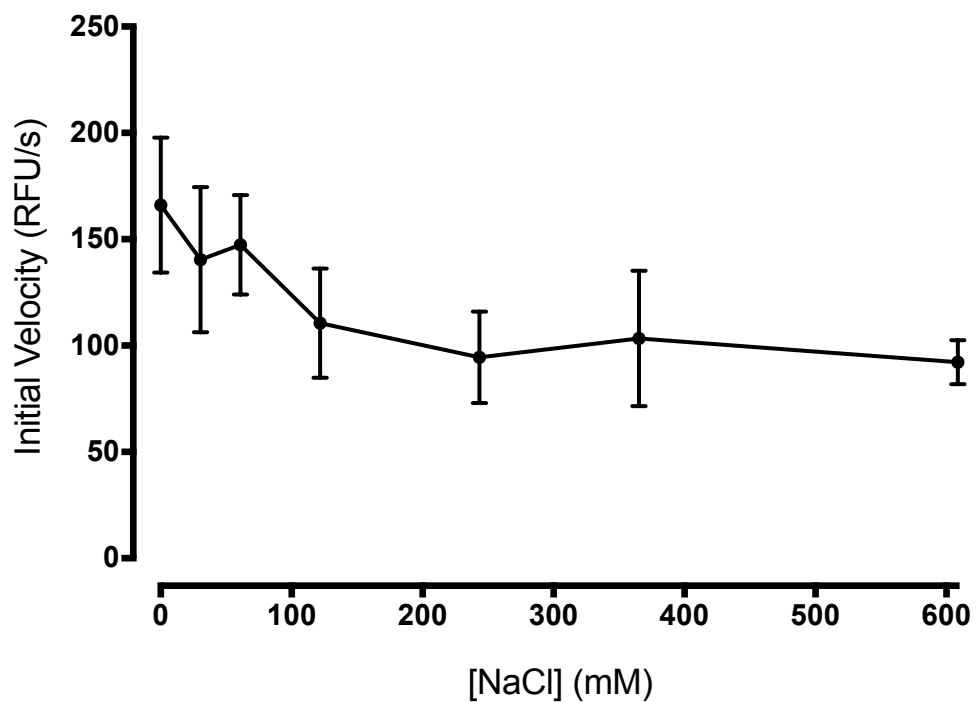


**Figure 4.4: Effect of NaCl.**

Assays were performed with various amounts of NaCl added. The initial velocity of each reaction was determined and plotted versus the concentration of NaCl in the reaction. No added NaCl gave the highest initial velocity, with decreasing activity with increasing amounts.

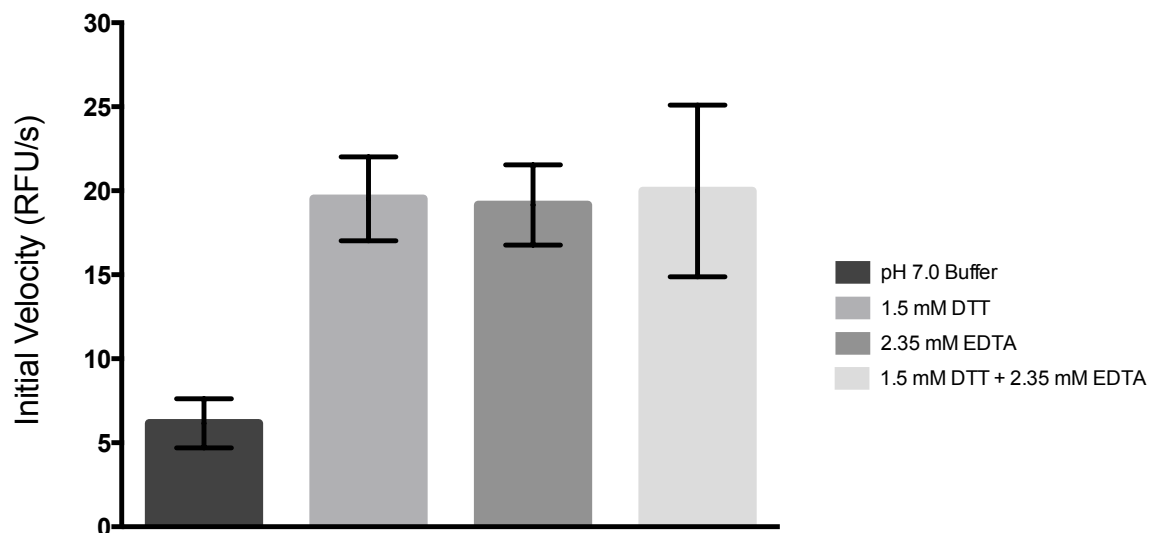


**Figure 4.5: Additive effects of pH 7.0 buffer with DTT and EDTA.**

Assays were performed in pH 7.0 buffer alone, pH 7.0 buffer with 1.5 mM DTT, pH 7.0 buffer with 2.35 mM EDTA, and pH 7.0 buffer with both 1.5 mM DTT and 2.35 mM EDTA. The initial velocity of each reaction was determined. The combination of DTT and EDTA gave a slightly higher initial velocity than either alone, but the difference was not statistically significant.

## Chapter 5

### Enzyme Kinetics of Wild-type Prp, Competition Assays with Alternative Substrates, and Activity of Active-site Mutants

Once the standard conditions for the fluorogenic peptide cleavage assay were established, this assay was used to determine the enzyme kinetics of wild-type Prp. Assays were performed at a constant enzyme concentration of 21.38 nM with fluorogenic substrate concentrations ranging from 0.2 to 2.0  $\mu\text{M}$ . Raw assay data were corrected for background with respect to no-enzyme blank reactions and then converted to concentration of substrate cleaved using the equation of a standard curve (Figure 2.1). Initial velocities were calculated for each substrate concentration and the results were entered into Prism<sup>®</sup>. The data were then fit to non-linear regression equations for Michaelis-Menten kinetics (1) and  $k_{\text{cat}}$  (2):

$$v_0 = \frac{v_{\text{max}}[S]}{K_m + [S]} \quad (1)$$

$$v_0 = \frac{[E_T]k_{\text{cat}}[S]}{K_m + [S]} \quad (2)$$

where  $v$  is initial velocity at a specific substrate concentration,  $v_{\text{max}}$  is the maximum velocity of the enzyme,  $[S]$  is the substrate concentration,  $K_m$  is the substrate concentration at one-half  $v_{\text{max}}$ ,  $[E_T]$  is the total concentration of enzyme active sites

(constrained to 42.765 nM active sites), and  $k_{\text{cat}}$  is the turnover number.

Results from these analyses are shown in Figure 5.1. The maximum velocity for cleavage of the fluorogenic substrate was determined to be  $1.960 \pm 0.060$  nM/s, the  $K_m$  was  $0.1824 \pm 0.0280$   $\mu\text{M}$ , the turnover number ( $k_{\text{cat}}$ ) was  $0.0458 \pm 0.0014$   $\text{s}^{-1}$ , and the specificity constant ( $k_{\text{cat}}/K_m$ ) was  $0.2511 \pm 0.0393$   $\mu\text{M}^{-1}\text{s}^{-1}$ .

Prp is also known to cleave the N-termini of *S. aureus* bacteriophage 80 $\alpha$  scaffold and major capsid proteins (Wall et al., 2015). Based on this information, we wanted to assess the substrate specificity of wild-type Prp. We ordered competitive peptides of various lengths (Table 3), based on the conserved L27 and 80 $\alpha$  major capsid protein cleavage motifs, and used these in the fluorogenic peptide cleavage assay. These assays will help determine what length of peptide is required for proper cleavage and whether Prp has higher affinity for one substrate over another. Assays were performed with each of the competitive peptides at 0.8  $\mu\text{M}$  with 0.2  $\mu\text{M}$  fluorogenic substrate and 21.38 nM enzyme. The raw data were treated identically to the kinetic data and the initial velocity for each reaction was used to calculate the percent inhibition with respect to a fluorogenic-peptide-only (no inhibitor) control. The initial velocity and percent inhibition for each inhibitor were then compared to the no-inhibitor control via an ordinary one-way ANOVA analysis with a p-value of 0.05.

All of the initial velocities and calculated percent inhibitions were significantly different from the no-inhibitor control. The results in Figure 5.2 show that the 13-mer based on the 80 $\alpha$  major capsid protein cleavage motif (CP13mer) causes more inhibition than a peptide identical to the fluorogenic peptide (without the fluorophore and

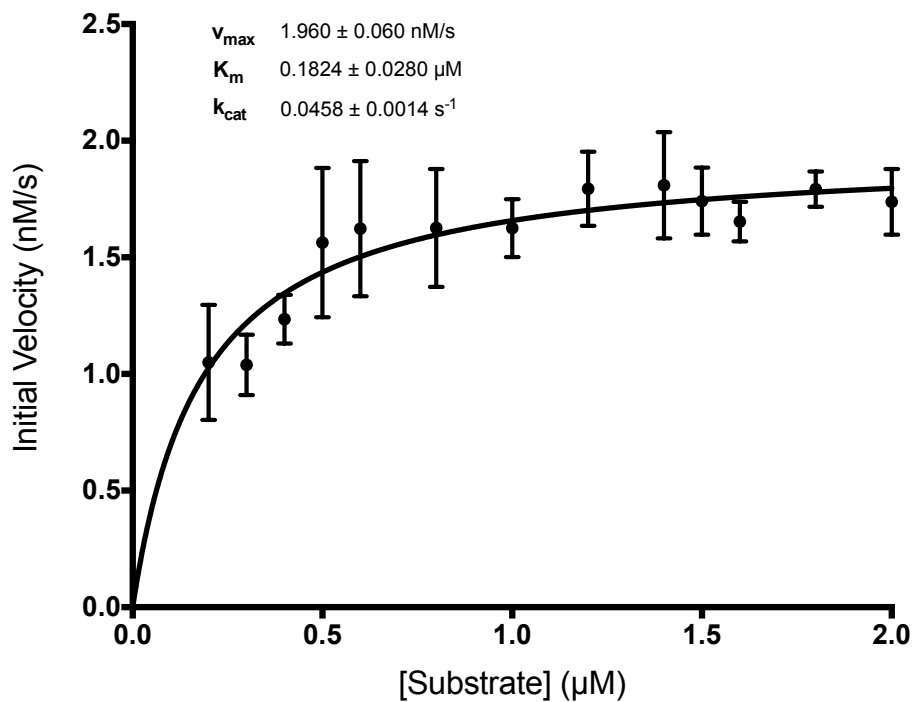


**Figure 5.1: Michaelis-Menten plot of Prp kinetics data.**

The average initial velocity at each substrate concentration was plotted. Based on fits to non-linear regression equations for Michaelis-Menten kinetics and  $k_{\text{cat}}$ , the  $v_{\max}$  was  $1.960 \pm 0.060$  nM/s, the  $K_m$  was  $0.1824 \pm 0.0280$   $\mu\text{M}$ ,  $k_{\text{cat}}$  was  $0.0458 \pm 0.0014$   $\text{s}^{-1}$ , and the specificity constant ( $k_{\text{cat}}/K_m$ ) was  $0.2511 \pm 0.0393$   $\mu\text{M}^{-1}\text{s}^{-1}$ .

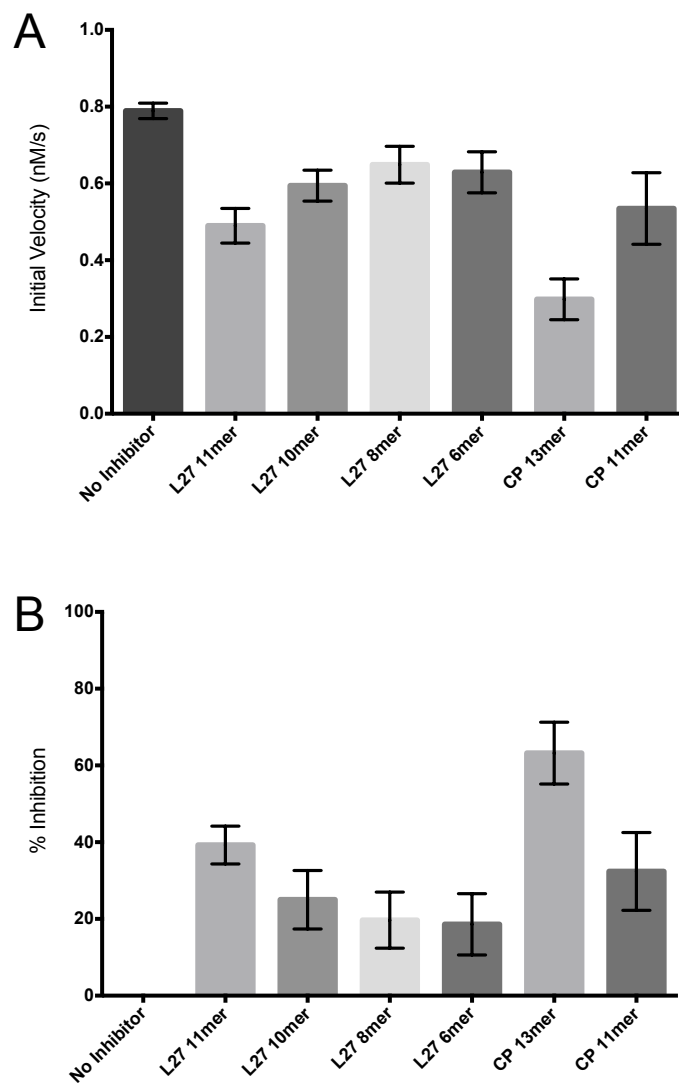


**Figure 5.2: Initial velocity and percent inhibition of assays with competitive peptides.**

(A) The average initial velocity for reactions containing 0.8  $\mu\text{M}$  of each inhibitor. (B) The percent activity for each peptide were calculated relative to the no-inhibitor control and converted to average percent inhibition.

quencher pair; L27 11mer). These data also show that peptides of longer length generally cause more inhibition than their shorter counterparts.

After determining the kinetics of the wild-type enzyme and testing several competitive peptides, the activity of several active-site mutants was tested and compared to that of the wild-type enzyme. Wild-type Prp and the mutants S38A, D31A, H22A, G21A, and C34S were assayed at 21.38 nM with 2.0  $\mu$ M fluorogenic substrate. Figure 5.3 shows that none of the mutants had any measureable activity at these concentrations. To determine if higher concentrations of mutant enzyme would produce any measureable activity, 213.8 nM of each enzyme was tested with 2.0  $\mu$ M substrate. Of these reactions, the S38A mutant had slight activity, measuring just  $2.06 \pm 0.22\%$  activity relative to the wild-type enzyme (Figure 5.4). These results indicate that all of the mutations made in Prp were detrimental to substrate binding, catalysis, or both.

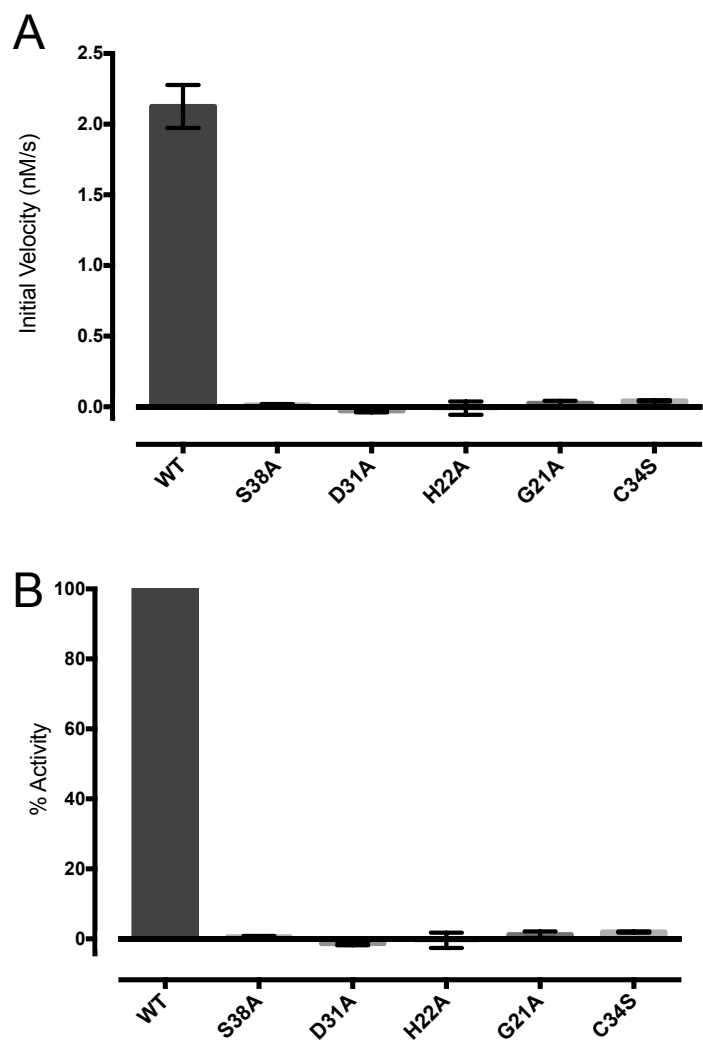


**Figure 5.3: Initial velocity and percent activity of Prp active-site mutants.**

(A) The average initial velocity for assays with each mutant. (B) The average percent activity for each mutant relative to the wild-type enzyme.



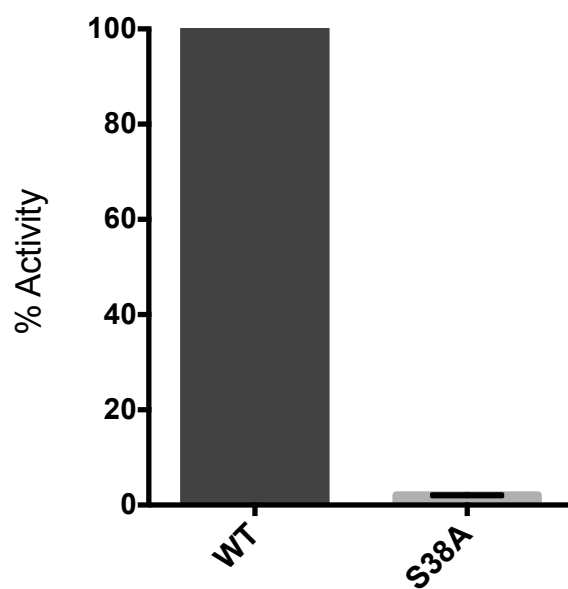


**Figure 5.4: Percent activity of S38A mutant.**

The average percent activity of the S38A mutant relative to the wild-type enzyme for reactions containing 10X more enzyme than usual (213.8 nM). The percent activity of the S38A mutant measured just  $2.06 \pm 0.22\%$  relative to wild-type.

## Chapter 6

### Discussion

Phage-related ribosomal protease is a 23.4 kDa dimer composed of two identical chains of 106 amino acids. Each of its monomers has two  $\alpha$ -helices, which form a two-layer  $\alpha/\beta$  sandwich with a five-strand, antiparallel  $\beta$ -sheet. This interface creates a cleft between the first  $\alpha$ -helix and second  $\beta$ -strand that contains several highly conserved residues, including a completely conserved cysteine and histidine, which constitute the proposed catalytic dyad of this protease. The dimer interface is formed between the two sets of  $\alpha$ -helices and is flanked by the two  $\beta$ -sheets on opposite sides. This protease has been classified by the MEROPS database into a new family, C108, which includes a protein of unknown function, TM1457, from *Thermatoga maritima* and a prohead protease from pneumococcal bacteriophage Cp-1 (Shin et al., 2005; Chirgadze et al., 2014; Rawlings et al., 2014; Wall, 2015). Based on a protein characteristics calculator, its approximate net charge at pH 7.0 is -27.1, its approximate isoelectric point is 4.07, and its approximate extinction coefficient is  $10,240 \text{ M}^{-1} \text{ cm}^{-1}$  (Innovagen). This protein has been shown to perform a novel, site-specific processing of ribosomal protein L27 in *S. aureus* (and the scaffold and major capsid proteins of staphylococcal phage 80 $\alpha$ ).

L27 is a component of the large (50S) ribosomal subunit and has been found to be in close proximity to the peptidyl transferase center (Lotti et al., 1987). It is composed

of a globular domain, which is a  $\beta$ -barrel-sandwich hybrid consisting of two sets of four-stranded  $\beta$ -sheets around a hydrophobic core, and an unstructured N-terminal region that has been shown to form an extended tail (Figure 1.4) (Wang et al., 2004). L27 has been shown to be necessary for efficient peptide bond formation and to be important for 50S subunit assembly; its deletion leads to impaired cell growth and partially assembled 50S subunit precursors (Wower et al., 1998). The N-terminal tail of L27 in *E. coli* extends into the peptidyl transferase center and its first three residues (AHK) have been shown to be important for peptidyl transferase activity, possibly helping to correctly position and stabilize tRNA in the PTC (Maguire et al., 2005; Voorhees et al., 2009). We have found that in *S. aureus* and related bacteria, L27 is encoded with a conserved N-terminal extension of nine amino acids, which occludes those residues shown to contribute to peptidyl transferase activity. Most bacteria with this extension encode a conserved gene encoding the protease responsible for its cleavage, which is not present in bacteria without this extension (Figure 1.5) (Spilman et al., 2012; Wall et al., 2015). This cleavage event has been shown to be essential to cell survival; pre-cleaved and un-cleavable variants could not complement a chromosomal deletion of L27 (Figure 1.6) (Wall, 2015).

All sequenced Firmicutes, Fusobacteria, and Synergistetes, as well as some Thermoactinomyces and Tenericutes have been found to encode N-terminally extended L27 along with a Prp homolog (Wall et al., 2015). This includes many well-known pathogens, several of which have been identified in national reports for their increasing prevalence of antibiotic resistance. In 2013, the Centers for Disease Control and Prevention (CDC) released an Antibiotic Resistance Threat Report listing several tiers of threats from

antibiotic resistant organisms. In this report, they list *Clostridium difficile* as an urgent threat (the highest level); while vancomycin-resistant *Enterococcus*, methicillin-resistant *S. aureus*, and drug-resistant *Streptococcus pneumoniae* are listed as serious threats; and vancomycin-resistant *S. aureus* is listed as a concerning threat (the lowest level) (CDC, 2013). Each of these organisms has been found to encode an L27 protein with the conserved N-terminal extension along with a homolog of Prp (Figure 1.5). This conservation suggests that with properly designed inhibitors, targeting the action of Prp could be an important and novel mechanism for helping to control these pathogens.

In this study, we have sought to determine the enzyme kinetics of wild-type Prp, test its substrate specificity using competitive peptide substrates, and test predictions made based on a structural model by generating and testing the activity of several active-site mutants. The results from this work provide insight into the basic functions of this enzyme while laying the groundwork necessary for the discovery of specific inhibitors via high-throughput screening.

The first steps in this study were the expression and purification of wild-type Prp. In order to simplify protein expression, we used autoinduction media, which relies on a metabolic switch from fermentation of glucose to lactose when growing cells reach a critical density. This switch induces high-level target-protein expression from the *T7lac* promoter and generally yields higher amounts of protein than conventional IPTG induction (Studier, 2005). After expressing Prp, we removed its His<sub>6</sub>-SUMO tag and purified the tagless protein. We found that the most efficient route involved an initial purification of the His<sub>6</sub>-SUMO-tagged protein via nickel affinity chromatography, followed by dialysis to remove the elution buffer. The purified fusion protein was then

cleaved with His<sub>6</sub>-tagged Ulp1, removing the His<sub>6</sub>-SUMO tag and leaving unmodified Prp. The mixture of His<sub>6</sub>-tagged Ulp1, the His<sub>6</sub>-SUMO tag, and tagless Prp was then run on another nickel affinity column and the tagless protein was eluted directly from the column, while the His<sub>6</sub>-SUMO tag and His<sub>6</sub>-tagged Ulp1 remained bound. This method provided a pure sample of Prp and was subsequently used to purify each of the active-site mutants (Figure 3.2).

After determining the concentration of wild-type Prp via Bradford assay and preparing a 40% glycerol freezer stock, a fluorogenic peptide cleavage assay was optimized. Several trial assays were performed to determine the appropriate settings for the plate reader, and then assays were performed to optimize the pH and concentrations of DTT, EDTA, and sodium chloride. The highest initial velocity was found at pH 7.0 with 1.5 mM DTT and 2.35 mM EDTA (Figure 4.5); therefore, these conditions were used for all subsequent assays.

To determine the kinetics of the Prp cleavage reaction, assays were performed with 0.2-2.0  $\mu\text{M}$  substrate and 21.38 nM enzyme. A standard curve (Figure 2.1) was used to convert the raw RFU values to concentration of substrate cleaved and the initial velocities were calculated using the linear portion of the curve for each reaction. These data were then fit to non-linear regression equations for Michaelis-Menten kinetics and  $k_{\text{cat}}$ . The maximum velocity ( $v_{\text{max}}$ ) for cleavage of the fluorogenic substrate was determined to be  $1.960 \pm 0.060$  nM/s, the  $K_{\text{m}}$  was  $0.1824 \pm 0.0280$   $\mu\text{M}$ , the turnover number was  $0.0458 \pm 0.0014$   $\text{s}^{-1}$ , and the specificity constant ( $k_{\text{cat}}/K_{\text{m}}$ ) was  $0.2511 \pm 0.0393$   $\mu\text{M}^{-1}\text{s}^{-1}$  (Figure 5.1).

We compared the kinetic parameters of Prp with those of Tobacco Etch Virus nuclear inclusion A protease (TEV Nla) (Table 4). This protease is another sequence-specific cysteine protease that has been well characterized. It cleaves at a conserved sequence of seven amino acids, ExxYxQ\*(S/G) (where \* denotes the cleavage site), and is used to separate constituents of the 364-kDa TEV polyprotein (Parks et al., 1995). Both Prp and TEV Nla have comparable specific activity (0.2325 vs. 0.38  $\mu\text{mol min}^{-1} \text{mg}^{-1}$ ). However, the  $K_m$  of Prp is about 400 times lower than TEV Nla, indicating that it has much higher affinity for its substrate. Also, the specificity constant ( $k_{\text{cat}}/K_m$ ) is higher for Prp. This could be due to the fact that the consensus sequence for Prp has more conserved residues and is slightly longer than that of TEV Nla, which may allow better recognition. Although the affinity and specificity of Prp is higher than TEV Nla, its turnover ( $k_{\text{cat}}$ ) is not as rapid, which could be due to its higher binding affinity, which must also be overcome to release its products. This kinetics profile provides information that will be useful during future high-throughput screening for inhibitors.

To next determine the substrate specificity of Prp, competitive peptides were included in assays with the fluorogenic substrate. These peptides ranged in length from 6-13 amino acids and were derived from either the L27 cleavage sequence or the sequence from staphylococcal phage 80 $\alpha$  major capsid protein (Table 3). Each of these peptides was added at 0.8  $\mu\text{M}$  into assays with 0.2  $\mu\text{M}$  fluorogenic substrate and 21.38 nM enzyme. An ordinary one-way ANOVA analysis of the initial velocity and percent inhibition from each assay indicated that each of the peptides caused significant inhibition compared to a no-inhibitor control (Figure 5.2). There was a visible trend in

**Table 4. Comparing the kinetics of sequence-specific proteases**

	<b>Phage-relate Ribosomal Protease (Prp)</b>	<b>Tobacco Etch Virus (TEV) Nuclear Inclusion A (NIa) Protease*</b>
<b>Sp. Activity</b> ( $\mu\text{mol min}^{-1} \text{mg}^{-1}$ )	0.2352 $\pm$ 0.0072	0.38
<b>K<sub>m</sub></b> ( $\mu\text{M}$ )	0.1824 $\pm$ 0.0280	69 $\pm$ 24
<b>k<sub>cat</sub></b> ( $\text{s}^{-1}$ )	0.0458 $\pm$ 0.0014	0.18 $\pm$ 0.022
<b>k<sub>cat</sub>/K<sub>m</sub></b> ( $\mu\text{M}^{-1} \text{s}^{-1}$ )	0.2511 $\pm$ 0.0393	0.0026
<b>Substrate</b>	KLNLQFF'ASKK	PTTENLYFQ'SGTVDRR
<b>Consensus Sequence</b>	KLXNLQXF'A	EXXYXQ'(S/G)

\* Parks et al., 1995

X indicates non-conserved amino acid

' indicates cleavage site

inhibition, with longer peptides causing more inhibition than their shorter counterparts. While the 13-mer based on the 80 $\alpha$  major capsid protein motif (CP 13mer) caused the greatest amount of inhibition (63.22%), there was no peptide from the L27 sequence that was directly comparable. Meanwhile, the 11-mer based on the L27 cleavage sequence showed similar inhibition to the 11-mer based on the 80 $\alpha$  major capsid protein sequence (39.26% vs. 32.38%). It is difficult to make conclusions based on these results with respect to which sequence Prp preferentially cleaves. By ordering peptides of matching length (both before and after the cleavage site) based on each of these motifs (including the 80 $\alpha$  scaffold protein motif) we would be able to make a more comprehensive evaluation of its specificity with respect to these different substrates. Another possible route would be to order the different peptides with fluorophore-quencher pairs and test them in individual kinetics assays. The respective kinetics data could then be used to compare the affinity of Prp towards the various substrates to determine which sequence is preferentially cleaved. While these results are inconclusive with respect to specificity, they do provide information that will be useful for inhibitor design. We have shown that Prp preferentially binds longer sequences; therefore, it is unlikely that a small, sequence-based inhibitor will be effective. On the other hand, because such a large recognition sequence seems to be required, a molecule that binds to or blocks somewhere along the binding site could prove to be an effective inhibitor.

Our lab has generated an active-site model of Prp based on an existing, incomplete crystal structure of Prp from *S. aureus* (Figure 6.1). This structure was



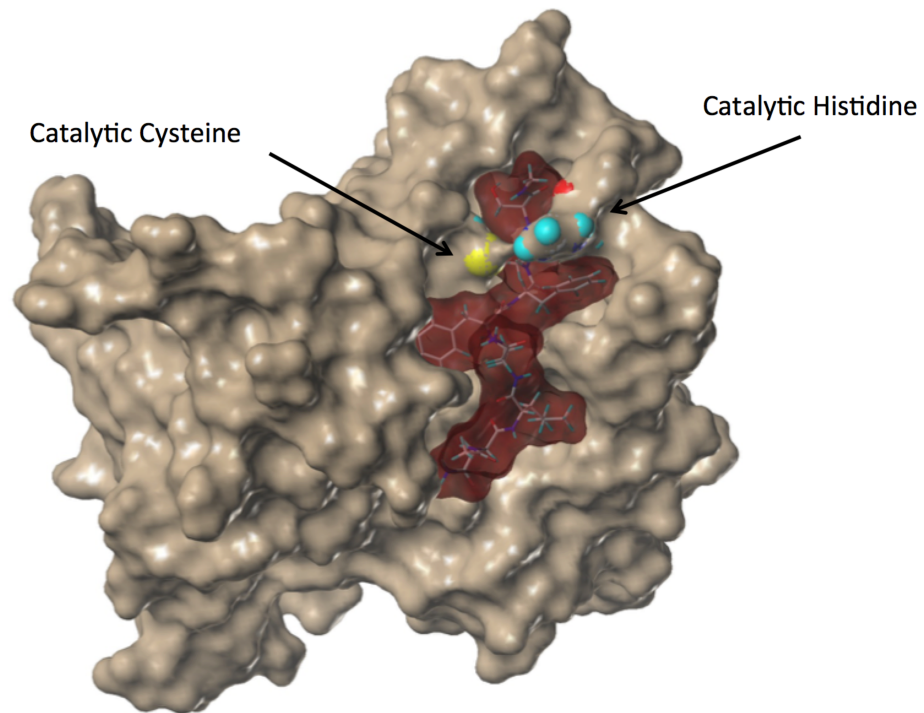


**Figure 6.1: Prp model with substrate docked.**

A molecular model of the Prp dimer (tan) built from an existing, incomplete crystal structure of Prp from *S. aureus*. A flexible loop between residues 21 and 32 was built back into the model, and a seven amino acid-long substrate (NLQFFAS; red) was docked at the active site. The catalytic cysteine and histidine are labeled (Adapted from Wall, 2015).

lacking a flexible loop that included the catalytic histidine, which had to be built back into the model (Wall, 2015). It was hypothesized that this flexible loop was important for substrate binding, and likely contributed to the formation of the active site. We have docked a seven amino acid-long substrate (Figure 6.1, red) into the active site of the Prp model and have identified several conserved residues that may play a role in substrate binding and catalysis (Wall, 2015). Figure 6.2 shows an atomic resolution model with residues FFAS of the substrate docked at the active site. Based on these models, we have chosen to mutate the catalytic cysteine (C34) and histidine (H22); the completely conserved glycine 21 and aspartic acid 31; and the partially conserved serine 38. Our model predicts  $\pi$ - $\pi$  stacking between the P1 phenylalanine ring of the substrate and the catalytic histidine. This interaction likely stabilizes the catalytic conformation of H22, which is predicted to be mobile due to its location on a flexible loop. This histidine is preceded on the loop by a completely conserved glycine that likely forms a hinge that allows for its movement. Aspartic acid 31 is found at the other end of the flexible loop and may be involved in substrate stabilization in the binding pocket. Finally, serine 38 seems to hydrogen bond with the amide nitrogen between the P2 and P1 phenylalanines of the substrate, which seems to orient the backbone in a way that promotes a split conformation between them, positioning them both in hydrophobic pockets. Each of these residues was changed to alanine, except for the catalytic cysteine, which was replaced with serine.

These mutants were expressed and purified identically to the wild-type enzyme, and surprisingly, in initial assays with 21.38 nM of each enzyme and 2.0  $\mu$ M fluorogenic

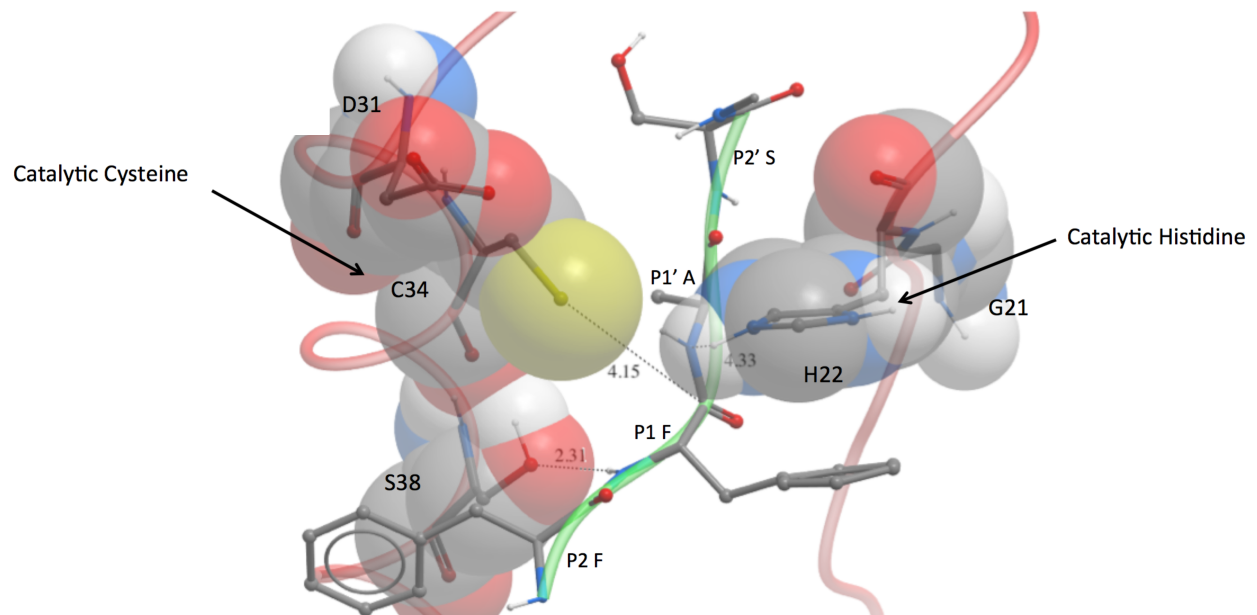


**Figure 6.2: Atomic resolution model of Prp active site with substrate docked.**

An atomic resolution model of the active site of Prp with residues FFAS of the substrate (ball-and-stick model with green backbone) docked (active-site residues shown as space-filling atoms over ball-and-stick models with red backbone). The catalytic cysteine (C34) and histidine (H22) are labeled, as well as residues G21, D31, and S38 (Adapted from Wall, 2015).

substrate, none of the mutants showed any measurable activity (Figure 5.3). After adjusting the concentration of the enzyme to 213.8 nM and keeping the same amount of substrate, only the S38A mutant showed slight activity; just  $2.06 \pm 0.22\%$  relative to the wild-type enzyme. We expected some of these mutants to have less dramatic effects and to be able to determine and compare the kinetics of each mutant. However, the results showed that they were all highly detrimental to substrate binding, catalysis, or both. We knew that mutating the cysteine and histidine would prevent catalysis and used them as controls along with the wild-type enzyme. The lack of activity in the glycine mutant shows that flexibility of the loop is critical and may be required for the histidine to adopt its catalytic conformation. The very low activity of the serine mutant shows that its stabilization of the substrate is very important for proper catalysis, and the effect of mutating the aspartic acid could be due to the presence of a catalytic triad, rather than a dyad, which would call for further refinement of our active-site model. Based on this information we are working on new models and are currently pursuing a crystal structure of Prp with its substrate bound, which will provide more in depth information about substrate binding and catalysis.

In this study, we have sought to characterize a novel cysteine protease that performs the essential, site-specific N-terminal processing of ribosomal protein L27 in *S. aureus* and related bacteria. We expressed and purified the wild-type enzyme and optimized an assay for its activity. Using this assay, we determined the kinetics of Prp and found that it has high affinity and specificity for its substrate, which may lead to its relatively slower rate of turnover. We then determined the substrate specificity of Prp and found that it prefers longer substrates, which has implications for inhibitor design.

Finally, we generated several active-site mutants to test predictions made based on our structural models. We found that the flexible loop at the active site is important for its catalytic conformation, that glycine 21 may be involved in the proper positioning of H22 for catalysis, that serine 38 seems to be important for substrate binding and stability, and that aspartic acid 31 may be part of a catalytic triad.

Future directions for this work include further examination of the substrate specificity of Prp, revisiting the role of aspartic acid 31 in the active-site model, generating a crystal structure for Prp with its substrate bound, using the optimized assay in high-throughput screening for inhibitors, and determining the cross-reactivity of Prp between species. The information gained from this and future studies will result in better understanding of this ribosomal protein-processing event and will aid in the design of new antibiotics that target this conserved, essential protease in *S. aureus* and related bacteria.

## References

- Bisswanger, H. (2014). Enzyme Assays. *Perspectives in Science*, 1, 41–55.
- Bush, K. (2011). Introduction to Antimicrobial Therapeutics Reviews: Antibiotics that target the ribosome. *Annals of the New York Academy of Sciences: Antimicrobial Therapeutics Reviews*, 1241, vii–ix.
- Centers for Disease Control and Prevention (CDC). Antibiotic resistance threats in the United States, 2013. Atlanta: CDC; 2013. Available from: <http://www.cdc.gov/drugresistance/threat-report-2013/pdf/ar-threats-2013-508.pdf>
- Chambers, H.F., & DeLeo, F.R. (2009). Waves of resistance: *Staphylococcus aureus* in the antibiotic era. *Nature Reviews-Microbiology*, 7, 629–641.
- Chaudhuri, R.R., Allen, A.G., Owen, P.J., Shalom, G., Stone, K., Harrison, M., Burgis, T.A., Lockyer, M., Garcia-Lara, J., Foster, S.J., Pleasance, S.J., Peters, S.E., Maskell, D.J., & Charles, I.G. (2009). Comprehensive identification of essential *Staphylococcus aureus* genes using Transposon-Mediated Differential Hybridisation (TMDH). *BMC Genomics*, 10(291).
- Chirgadze, Y.N., Clarke, T.E., Romanov, V., Kisselman, G., Wu-Brown, J., Soloveychik, M., Chan, T.S.Y., Gordon, T.D., Battaile, K.P., Pai, E.F., & Chirgadze, N.Y. (2015). The structure of SAV1646 from *Staphylococcus aureus* belonging to a new 'ribosome-associated' subfamily of bacterial proteins. *Acta Crystallographica Section D Biological Crystallography*, 71(2), 332–337.
- Coates, A., Hu, Y., Bax, R., & Page, C. (2002). The future challenges facing the development of new antimicrobial drugs. *Nature Reviews-Drug Discovery*, 1, 895–910.
- Cole, S.T. (2014). Who will develop new antibacterial agents?. *Philosophical Transactions of The Royal Society B*, 369, 1–7.
- Deu, E., Verdoes, M., & Bogoyo, M. (2012). New approaches for dissecting protease functions to improve probe development and drug discovery. *Nature Structural & Molecular Biology*, 19(1), 9–16.

- Drag, M., & Salvesen G.S. (2010). Emerging principles in protease-based drug discovery. *Nature Reviews-Drug Discovery*, 9, 690–701.
- Dubendorff, J. W., & Studier, F. W. (1991). Controlling basal expression in an inducible T7 expression system by blocking the target T7 promoter with lac repressor. *Journal of Molecular Biology*, 219(1), 45–59.
- Fischbach, M.A., & Walsh, C.T. (2009). Antibiotics for emerging pathogens. *Science*, 325, 1089–1093.
- Gordon, R.J., & Lowy, F.D. (2008). Pathogenesis of methicillin-resistant *Staphylococcus aureus* infection. *Clinical Infectious Diseases*, 46(Suppl. 5), S350–S359.
- Hammond, J. B., & Kruger, N. J. (1988). The Bradford method for protein quantitation. *Methods in Molecular Biology (Clifton, N.J.)*, 3, 25–32.
- Hermann, T. (2005). Drugs targeting the ribosome. *Current Opinion in Structural Biology*, 15, 355–366.
- Innovagen.se., 'Peptide Property Calculator - Calculate MW (Molecular Weight), Pi (Iso-Electric Point), Net Charge, Titration Curve (Charge Vs Ph), Hydrophilicity, Hydrophobicity - Find Out Physicochemical Properties Of Your Peptide!'. N.p., 2015. Web. 3 July 2015.
- Kreiswirth, B.N., Löfdahl, S., Betley, M.J., O'Reilly, M., Schlievert, P.M., Bergdoll, M.S., & Novick, R.P. (1983). The toxic shock syndrome exotoxin structural gene is not transmitted by a prophage. *Nature*, 305, 709–712.
- Ligozzi, M., & Fontana, R., (2003). Isolation of total DNA from bacteria and yeast. *African Journal of Biotechnology*, 2(8), 251–253.
- Lotti, M., Stöffler-Meilicke, M., & Stöffler, G. (1987). Localization of ribosomal protein L27 at the peptidyl transferase centre of the 50S subunit, as determined by immune-electron microscopy. *Molecular Genetics and Genomics*, 210, 498–503.
- Lowy, F.D. (1998). *Staphylococcus aureus* Infections. *The New England Journal of Medicine*, 339(8), 520–532.
- Lowy, F.D. (2003). Antimicrobial resistance: the example of *Staphylococcus aureus*. *The Journal of Clinical Investigation*, 111(9), 1265–1273.
- Maguire, B.A., Beniaminov, A.D., Ramu, H., Mankin, A.S., & Zimmermann, R.A. (2005). A protein component at the heart of an RNA machine: the importance of protein L27 for the function of the bacterial ribosome. *Molecular Cell*, 20, 427–435.

- Malakhov, M. P., Mattern, M. R., Malakhova, O. A., Drinker, M., Weeks, S. D., & Butt, T. R. (2004). SUMO fusions and SUMO-specific protease for efficient expression and purification of proteins. *Journal of Structural and Functional Genomics*, 5, 75–86.
- Parks, T.D., Howard, E.D., Wolpert, T.J., Arp, D.J., & Dougherty, W.G. (1995). Expression and purification of a recombinant Tobacco Etch Virus NIa proteainse: Biochemical analyses of the full-length and a naturally occurring truncated proteinase form. *Virology*, 210, 194–201.
- Peracchi, A. (2001). Enzyme catalysis: removing chemically ‘essential’ residues by site-directed mutagenesis. *TRENDS in Biochemical Sciences*, 26(8), 497–503.
- Poehlsgaard, J., & Douthwaite, S. (2005). The bacterial ribosome as a target for antibiotics. *Nature Reviews-Microbiology*, 3, 870–881.
- Poliakov, A., Chang, J.R., Spilman, M.S., Damle, P.K., Christie, G.E., Mobley, J.A., & Dokland, T. (2008) Capsid size determine by *Staphylococcus aureus* Pathogenicity Island 1 SaPI1 involves specific incorporation of SaPI1 proteins into procapsids. *Journal of Molecular Microbiology*, 380, 465–475.
- Pribnow, D. (1975). Bacteriophage T7 early promoters: nucleotide sequences of two RNA polymerase binding sites. *Journal of Molecular Biology*, 99, 419–443.
- Rawlings, N. D., Waller, M., Barrett, A. J., & Bateman, A. (2014). MEROPS: The database of proteolytic enzymes, their substrates and inhibitors. *Nucleic Acids Research*, 42(D1), 503–509.
- Reyes-Robles, T., Alonzo III, F., & Torres, V.J. (2014). *S. aureus* virulence factors thwart host immune responses. *Microbe*, 9(6), 240–244.
- Roucourt, B., & Lavigne, R. (2009). The role of interactions between phage and bacterial proteins within the infected cell: a diverse and puzzling interactome. *Environmental Microbiology*, 11(11), 2789–2805.
- Shajani, Z., Sykes, M.T., & Williamson, J.R. (2011). Assembly of bacterial ribosomes. *Annual Review of Biochemistry*, 80, 501–526.
- Shin, D. H., Lou, Y., Jancarik, J., Yokota, H., Kim, R., & Kim, S. H. (2005). Crystal structure of TM1457 from *Thermotoga maritima*. *Journal of Structural Biology*, 152, 113–117.
- Shoji, S., Dambacher, C.M., Shajani, Z., Williamson, J.R., & Schultz, P.G. (2011). Systematic chromosomal deletion of bacterial ribosomal protein genes. *Journal of Molecular Biology*, 413, 751-761.



- Studier, F. W. (2005). Protein production by auto-induction in high density shaking cultures. *Protein Expression and Purification*, 41, 207–234.
- Studier, F. W., & Moffatt, B. A. (1986). Use of bacteriophage T7 RNA polymerase to direct selective high-level expression of cloned genes. *Journal of Molecular Biology*, 189, 113–130.
- Sweet, C. R. (2003). Expression of recombinant proteins from lac promoters. *Methods in Molecular Biology (Clifton, N.J.)*, 235, 277–288.
- Voorhees, R.M., Weixlbaumer, A., Loakes, D., Kelley, A.C., & Ramakrishnan, V. (2009). Insights into substrate stabilization from snapshots of the peptidyl transferase center of the intact 70S ribosome. *Nature Structural & Molecular Biology*, 16(5), 528–533.
- Wall, Erin A. 'Elucidation of a Novel Pathway In *Staphylococcus aureus*: The Essential Site-Specific Processing of Ribosomal Protein L27'. Ph.D. Virginia Commonwealth University, 2015. Print.
- Wall, E. A., Caufield, J. H., Lyons, C. E., Manning, K. A., Dokland, T., & Christie, G. E. (2015). Specific N-terminal cleavage of ribosomal protein L27 in *Staphylococcus aureus* and related bacteria. *Molecular Microbiology*, 95(2), 258–269.
- Wang, H., Takemoto, C.H., Murayama, K., Sakai, H., Tatsuguchi, A., Terada, T., Shirouzu, M., Kuramitsu, S., & Yokoyama, S. (2004). Crystal structure of ribosomal protein L27 from *Thermus thermophilus* HB8. *Protein Science*, 13, 2806–2810.
- Wertheim, H.F.L., Melles, D.C., Vos, M.C., van Leeuwen, W., van Belkum, A., Vergrugh, H.A., & Nouwen, J.L. (2005). The role of nasal carriage in *Staphylococcus aureus* infections. *The Lancet Infectious Diseases*, 5, 751–762.
- Wower, I.K., Wower, J., & Zimmermann, R.A. (1998). Ribosomal protein L27 participates in both 50S subunit assembly and the peptidyl transferase reaction. *The Journal of Biological Chemistry*, 273(31), 19847–19852.

## Vita

Adam Lee Johnson was born on July 27, 1989 in Norfolk, Virginia. He graduated from Kecoughtan High School, Hampton, Virginia in 2007 and received his Bachelor of Science in Chemistry and Biochemistry from Old Dominion University in 2012. He earned a Master of Science in Microbiology and Immunology from Virginia Commonwealth University in Richmond, Virginia in 2015.

### Abstracts and Presentations:

Johnson, A., Wall, E.A., Dokland, T., & Christie, G.E. Characterization of a Novel Protease in *Staphylococcus aureus*. American Society of Microbiology – Virginia Branch, James Madison University, Harrisonburg, VA. 2014. Presentation.

### Honors and Awards:

Charles C. Clayton Award (February 2015)  
Phi Kappa Phi Nomination Award (February 2015)